Texture Analysis and Classification of Vascular Plaque from Optical Coherence Tomography Images

by

Ammu Prakash

A Thesis submitted to the Faculty of Graduate Studies of

The University of Manitoba

in partial fulfilment of the requirements of the degree of

MASTER OF SCIENCE

Department of Electrical and Computer Engineering

University of Manitoba

Winnipeg

ACKNOWLEDGEMENTS

I would like to thank first and foremost my advisor, Dr. Sherif for all that I have learned from him and for his guidance throughout my masters program. His advice and encouragement were always important and helped me towards my personal and professional development. Whenever I had a hard time in many respects, he supported me to overcome the difficulties. I would also like to thank him for helping me to shape my interests and ideas.

Besides my advisor, I want to thank the rest of examinee committee: Dr. Arkady Major and Mark Hewko for their valuable comments, suggestions, and questions. My sincere thanks go to Mark Hewko and Mostaço-Guidolin Leila Büttner for helping me with data collections and data interpretations.

Next I would like to thank my friend Dr. Snehil Dua for her endless support and motivation throughout these years.

Finally I thank my parents, my brother, Arvind and my partner, Siddique, without their support it would not have been possible.

Table of Contents

List of tables

List of Figures

ABSTRACT

The ability to detect atherosclerotic plaque from optical coherence tomography (OCT) images by visual inspection is usually limited. We developed a texture based segmentation method using supervised and unsupervised classification to detect atherosclerotic plaque from OCT images without any reliance on visual inspection. Our Supervised method involves extraction of statistical textural features using the Spatial Gray Level Dependence Matrix (SGLDM) method, feature extraction and feature selection method, and application on supervised algorithm (*K-nn*). Our second method is based on unsupervised classification involves extraction of statistical textural features using the SGLDM method, application of an unsupervised clustering algorithm (*K-means*) on these features, and mapping of the segmented regions of features back to the actual image. We verified our results by visually comparing them to photographs of the vascular tissue with atherosclerotic plaque that we used to generate our OCT images. Our method could be potentially used in clinical cardiovascular OCT imaging.

CHAPTER 1: INTRODUCTION

Cardiovascular disease is one of the main causes of premature death in many countries, accounting 29% deaths in Canada annually [1], 4.35 millions of deaths each year in Europe, and 35% of death in the United Kingdom [2, 3]. Each year, about 250,000 potential years of life are lost in Canada due to cardiovascular diseases [4].This emphasizes the importance of detecting and diagnosing the conditions that cause such adverse cardiac events. The main cause of acute coronary syndromes and sudden cardiac death is Atherosclerosis. Atherosclerotic artery disease arises due to the accumulation of plaque inside the arteries. Over 60 % of myocardial infarctions and sudden cardiac deaths are caused due to atherosclerotic plaques [5]. Atherosclerosis is a process in which blood lipids such as cholesterol accumulate on artery walls. As cholesterol continues to deposit in artery walls, these fatty materials turn into plaques. This condition may eventually lead to narrowing or blocking of arteries.

There are several imaging modalities that can detect atherosclerosis. For coronary artery imaging, the imaging methods can be divided into two categories: invasive imaging and noninvasive imaging [6, 7]. Cardiac magnetic resonance and multi-detector x-ray computed tomography are the leading non-invasive techniques that have to potential to image vulnerable plaque. Invasive imaging mainly includes X-ray angiography, intravascular ultrasound (IVUS) and optical coherent tomography (OCT). Despite the advances in non-invasive imaging methods, the option to immediately invoke treatment ensures that catheterizations will continue to be relied upon clinically to locate and then treat target lesions. Invasive intravascular imaging will continue to play an important

role for as long as interventional strategies such as balloon angioplasty, stenting and atherectomy remain front-line treatments of the disease. Intravascular ultrasound (IVUS) imaging, introduced in the late 80s, produces circumferential tomographic images of the vessel wall. IVUS is capable of providing 3D anatomical information and is becoming increasingly used to assess plaque burden as well as guide and evaluate interventional catheterization procedures. Typical IVUS catheters operate between 20 – 40 MHz providing a 40 – 20 μm upper limit on the spatial resolution of the images. Practically, IVUS images have 2 to 5 times lower resolution than optical coherence tomography. Optical coherence tomography (OCT) is capable of achieving imaging resolution in the axial dimension on the 10 μm scale. The higher resolution available from IV-OCT systems is its primary advantage over the established IVUS technology. With the higher resolution available from IV-OCT, detailed anatomical features of the vessel wall and plaque are easily visualized compared to IVUS. The argument for using IV-OCT to guide interventional procedures is compelling as the high resolution afforded by IV-OCT enables monitoring of several risk factors associated with atherosclerosis.

1.1 Motivation

Cardiovascular disease is the leading cause of death and hospitalization in Canada. It accounts for approximately 32% of all deaths and 15% of total hospitalizations. 80% of Canadians have at least one risk factor for cardiovascular disease. These risk factors include smoking, alcohol, physical inactivity, obesity, diabetes, or high blood pressure or high cholesterol. While the death rates from cardiovascular disease declined 30% between 1994 and 2004, it still remains Canada's leading cause of death.

Cardiovascular disease (CVD) covers a wide range of diseases. Not all of them are directly due to atherosclerosis, but many of the major diseases are related to it. Major effects of atherosclerosis are myocardial infarction commonly referred to as a *heart attack*, cerebral infarction, also known as ischemic stroke, aortic aneurysms (abnormal bulging or swelling of a portion of a blood vessel), and peripheral vascular disease. Atherosclerosis can begin to develop very early in life starting from age 15 years onwards. The lesions that provoke the symptoms often are not stenotic, i.e., causing artery narrowing, and, thus, are not detectable by conventional contrast angiography. For this reason, the visualization and determination of the composition of vascular plaque is more important than the degree of stenosis.

Among all imaging modalities for coronary arteries, IVUS and OCT are currently the most capable in imaging the vessel's wall. OCT has a spatial resolution of 10-20 μm, which is ten times higher than the resolution of IVUS. Furthermore, using histological controls, it has been demonstrated that OCT is superior to IVUS, making OCT better suited for detecting important features of vulnerable plaque components, including thickness of fibrous cap, thrombus and density of macrophages [8- 10]. To our knowledge, texture segmentation of atherosclerotic plaque has not been previously performed on OCT images. However, a large body of literature exists for texture segmentation of atherosclerotic plaque using IVUS, magnetic resonance imaging (MRI) [11- 13].

1.2 Problem statement

The ability to detect atherosclerotic plaque from optical coherence tomography (OCT) images by visual interpretation is often limited and complicated by the high frame rate

of modern intravascular OCT systems. We developed a texture based segmentation method to detect atherosclerotic plaque from OCT images without reliance on visual ability. This method involves extraction of statistical textural features using spatial gray level dependence matrix (SGLDM) method, application of unsupervised and supervised learning using *K-means* clustering and *k-nn* algorithms and thereby detecting the plaque region on OCT images. We evaluated our results by comparing the obtained segmented results of atherosclerotic plaque with actual photographs of vascular tissue. The statistical properties of tissue can be well characterized using OCT images because of their higher resolution and because they frequently display a characteristic texture due to speckle [14]. Our texture based segmentation method using OCT images could be used to differentiate atherosclerotic plaque regions from healthy tissue regions.

This thesis aims to provide methods that could help speed up and/or increase the accuracy of the detection/ diagnosis of atherosclerosis disease.

1.3 Methodology

To address the stated problem and achieve our objectives, the following methods and techniques were used to automatically detect atherosclerotic regions:

1. Experimental set up

   We used an OCT system, at the Institute of Biodiagnostics, National Research Council Canada, in Winnipeg, to acquire images of vascular tissue. OCT is a minimally invasive imaging modality that provides cross sectional images. Among various OCT techniques, we used swept-source OCT system (SSOCT).

2. Animal model and tissue preparation (performed by colleagues at the Institute of Biodiagnostics, National Research Council Canada, Winnipeg)

We used myocardial infarction prone Watanabe heritable hyperlipidemic rabbits, referred as WHHLMI rabbits [15, 16] to obtain samples of vascular tissues with atherosclerotic plaque. Arterial samples harvested from seven WHHLMI rabbits aged 309, 316, 330, 332, 360, 450, 480, 577, 655 and 666 days were obtained. Segments of tissue starting from the ascending aorta to the external iliac artery were excised from all specimens and subdivided into 20~30 mm long sections. WHHL rabbits show hypercholesterolemia due to a deficiency of LDL receptors, and a very similar lipoprotein metabolism to humans [16].

3. Image preprocessing

Raw OCT images contained floating point numbers so we performed image normalization on each OCT vascular image file to achieve a uniform distribution of intensities on a standardized intensity range and to improve contrast. This was performed using a Min-Max normalization operation.

We also performed image segmentation using automatic thresholding technique to improve the image quality.

4. Feature generation and feature normalization

To generate the texture features on our processed OCT vascular images, we used SGLDM method. SGLDM is a well known method for extracting second order texture features. This method is based on an estimate of second-order joint conditional probability density functions p ($i, j: d, \theta$) [17-20]. These probability

density functions, p (*i, j: d, θ*), measure the probability that two pixels, which are located with an inter sample distance, *d* and direction, *θ*, have gray levels *i* and *j*. To detect the atherosclerotic plaque using these SGLDMs, we extracted 11 texture features in two directions with $d = 1$.

5. Unsupervised and supervised classification

   Pattern recognition/classification is a broad field that has developed to address problems such as face recognition, manufactured product inspection, speech recognition, and breast cancer screening etc. One major division is between supervised and unsupervised classification techniques. Supervised methods require that the classifications of the samples be known and provided to the classifier. Unsupervised methods, on the other hand, do not require *a priori* knowledge of sample classifications, *i.e.*, class labels are unknown. In this thesis, we performed both automatic supervised and unsupervised learning to classify plaque from normal tissue. To perform supervised classification, we employed a *K-nn* classifier. And to perform unsupervised classification, we designed a k_{means} clustering algorithm. In order to verify the results of our unsupervised classification, we compared our resulting segmented OCT images with different locations on photographic images of vascular tissue with atherosclerotic plaque.

1.4 Thesis outline

In chapter 2, an overview of atherosclerosis diseases and their development is provided. Also we presented how atherosclerosis is related to cardio vascular disease.

In chapter 3, the basic principles of OCT and SSOCT, and their applications are presented.

In chapter 4, an overview of pattern recognition /classification, texture feature generation technique using SGLDM, and the design of the supervised classifier to classify plaque and healthy tissue from vascular OCT images are explained.

In chapter 5, we describe the design of our unsupervised classifier to detect atherosclerotic regions from OCT vascular images. We validated our method and results by comparison with photographic images of vascular tissues.

Conclusions and suggestions for future work are included in chapter 6.

CHAPTER 2: ATHEROSCLEROSIS

2.1 Introduction

Cardiovascular disease continues to be a leading cause of morbidity and mortality around the globe, for both men and women [21]. It is estimated that cardiovascular diseases are responsible for 29% of deaths in Canada annually [1]. Atherosclerosis is mainly responsible for coronary heart disease, ischemic strokes, and peripheral vascular disease [22]. One of the main causes of acute coronary syndromes and sudden cardiac death is atherosclerosis. This chapter emphasizes background on atherosclerosis, development of Atherosclerotic plaque, signs and symptoms of Atherosclerosis, morphology of Atherosclerotic plaques, risk factors of atherosclerosis, different types of Atherosclerosis, literature review on imaging vascular plaque and the description of animal model we used in our study.

2.2 Background

The arteries blood vessels are susceptible to various diseases that can reduce blood flow, alter blood pressure and produce blood clot. Atherosclerosis is the most common and clinically significant of these diseases. Atherosclerosis is the derived from the greek word “athero” meaning porridge and refers to plaque . “Sclerosis” meaning hardening , refers to connective tissue of this disease [23]. Atherosclerosis is the specific form of arteriosclerosis. Arteriosclerosis means “hardening of the arteries”. Arteriosclerosis comprises of three patterns of vascular diseases. Atherosclerosis is one of these vascular

disease which thickens intima of the artery wall, which can cause luminal reduction and reduces blood flow.

Definition of Atherosclerosis: It is defined as chronic inflammatory fibro-proliferative (relating to the growth and proliferation of fibroblasts, the most basic connective tissue cell.) disease of arterial intima [24].

2.3 Development of Atherosclerosis

Atherosclerotic plaques can be characterized into stable plaque and unstable or vulnerable plaque. Vulnerable plaque is liable to complications and prone to rupture. Plaque rupture can also be called as the process underlying thrombus formation (formation of blood clot that forms within a blood vessel or inside the heart). Vulnerable plaques are formed when the fat droplets in the blood are absorbed by the artery. When an artery absorbs these fat droplets, it releases inflammation causing proteins (called Cytokeins). These Cytokeins make the artery's wall sticky, which then attracts immune system cells called monocytes. These monocytes squeeze into artery walls and absorb the fat droplets and thus block the blood flow in artery. This inflammatory process forms the vulnerable plaque. When this inflammation is combined with other factors such as high blood pressure, diabetes, it can cause plaque disruption. The disrupted plaque spills its contents into the bloodstream. The sticky cytokines on the artery wall captures blood cells. When these blood cells clump together, they could form a large clot and eventually block the artery.

The normal artery wall consists of three main layers that surround the arterial lumen (the part of artery where blood flows). The inner layer is called intima, the middle layer is called media and the outer layer is known as adventitia

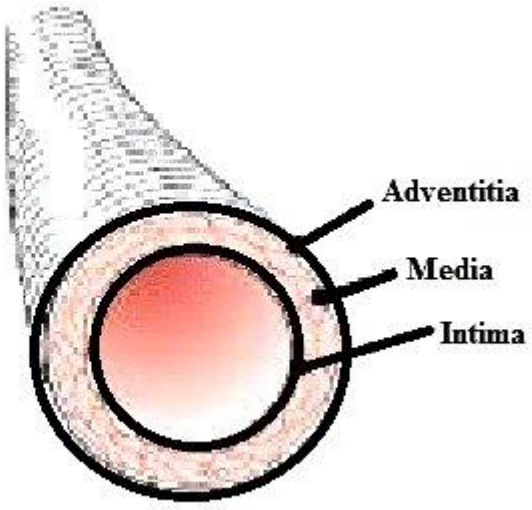

Figure 2.1 Three main layers of normal coronary artery

The intima, which is composed of a very thin layer in a normal artery, is separated from the lumen by a single layer of endothelial cells called as endothelium. This layer forms physical and functional barrier between the circulating blood in the lumen and tissue. This location, is the most likely to develop an atherosclerotic plaque.

Endothelial cell damage is the inital and most crucial lesion in the development of Atherosclerosis. A very high concentration of blood homocysteine (an amino acid) is known to damage endothelium and cause Atherosclerosis [25].

2.4 Signs and symptoms of Atherosclerosis

The earliest visible change of atherosclerosis is accumulation of lipid in the artery walls. These are flat and yellow fatty streaks, it indicates that the damaged endothelium has lost its ability to prevent passage of cholesterol into arterial wall [25]. Symptoms of atherosclerosis in many cases are clinically in apparent [26]. The first sign or symptom in many cases is heart attack or stroke. However people with significant atherosclerosis have history of increased cholesterol levels and may also experience angina.

2.5 Morphology of Atherosclerotic plaque

There has been studies based on coronary angiographic shows that plaque which is most likely to produce blood clot formation resulting in myocardial infraction (heart attack) causes stenosis (narrowing) of vessel of 10-40%. This type of plaques remains asymptomatic for years. They are characterized by large lipid rich surrounded by thin fibrous caps. Rupture can occur at the edges of thin fibrous caps and expose the lipid cores of plaques into the blood forming the blood clot that may totally block the blood flow [22]. When a coronary artery becomes completely blocked, and when there is no blood flow, myocardial infarction (Heart attack) occurs. Plaques with lipid rich cores and thin fibrous caps are more unstable than the stenotic plaques (plaques that narrows the vessel). Stenotic plaques are generally have thicker fibrous caps which makes them more stable and they generally do not cause myocardial infarction or death.

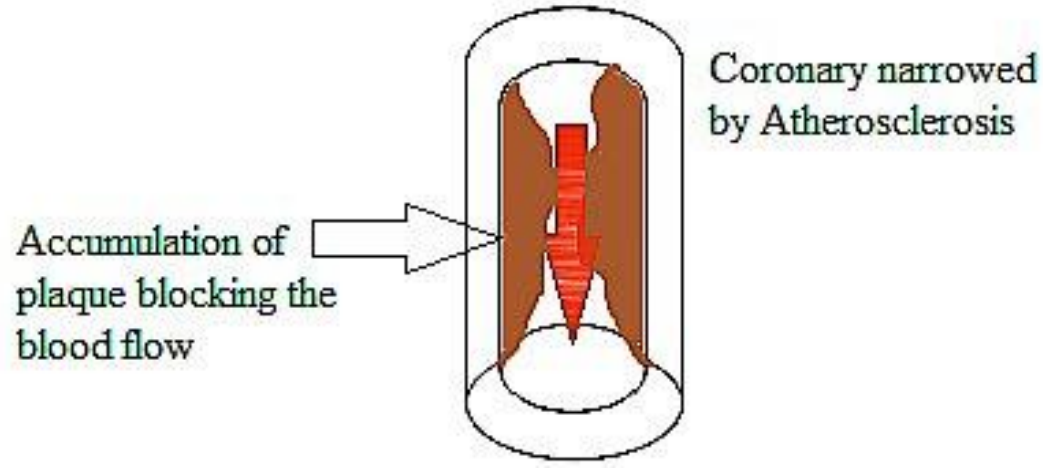

Figure 2.2. Advancing atherosclerosis where accumulating plaque results in a progressive narrowing of the vessel and blocks blood flow.

2.6 Risk factors of atherosclerosis:

A review article by Stocker and Keaney [27] summarizes risk factors that are strongly and consistently associated with cardiovascular disease.

AGE: Age is one of the most important risk factors. Atherosclerosis worsens steadily with increasing age. According to the American Heart Association about 82 % of people who have a coronary heart disease are 65 or older. At older ages, women are more likely than men to have heart attacks. From age 40-60, the number of heart attacks increases fivefold than in younger age groups [28].

GENDER: Gender is also an influential factor. A number of clinical studies have suggested that men are much more prone to develop atherosclerosis than women [29]. There have been speculations that estrogens may protect women, however there is no firm evidence supporting such speculations [30].

BLOOD CHOLESTROL: High level of low-density lipoprotein (LDL) is the most important risk factor for cardiovascular heart disease. LDL refers to class and range of lipoproteins which carry cholesterol in the blood. The risk of cardio vascular disease and other complications of atherosclerosis double with every 40 mg/dL rise of total LDL cholesterol level [30]. The WHO estimates that over 60% of cardio vascular disease in developed countries is due to excess of blood cholesterol level [32, 14].

HYPERTENSION: Hypertension can be defined as systolic blood pressure in excess of 140 mmHg or diastolic blood pressure above 90 mmHg. Patients with systolic blood pressure have five times more risk to atherosclerosis than those with normal blood pressure. There is a linear relation between blood pressure elevation and the increased risk of atherosclerosis [33].

SMOKING: Numerous observational studies show that smoking increases atherosclerotic disease by 50% (80% in heavy smokers) and doubles the risk of cardio vascular disease [34]. About half of all regular smokers will suffer a fatal myocardial infarction eventually [31]. Passive smoking also increases the risk of cardio vascular disease compared to nonsmokers [35]. Statistics shows that smokers have 70% greater risk of death from cardio vascular disease than nonsmokers [28].

DIABETES: In patients with diabetes the risk of cardio vascular disease is two–three folds greater than and twice as high in diabetic males and three times as high in diabetic females than non-diabetics. Diabetes not only increase the risk of cardio vascular disease but it also increases the effect of other risk factors associated with cardiovascular disease such as raised cholesterol levels, raised blood pressure, smoking and obesity. In diabetic people, coronary heart disease causes almost 60% of their deaths [36,37].Thus diabetes represents a major risk factor to atherosclerosis.

OBESITY: There has been substantial research effort that shows that obesity is associated with an increased risk of coronary heart disease [38]. It is likely that inflammation induced by obesity accelerates atherosclerosis [39]. Also, it has been estimated that 30% of cardiovascular disease in developed countries is related to physical inactivity [40]. The adverse effect of obesity is more pronounced when the fat is concentrated in the abdomen.

2.7 Types of Atherosclerotic lesions:

According to the American Heart Association, atherosclerotic lesions can be classified into the following 8 types:

Type I (Initial change lesion): This type of lesion is comprised of a small group of isolated macrophage foam cells (a large white blood cell, found primarily in the bloodstream and connective tissue, that helps the body fight off infections by ingesting the disease-causing organism) in the sub endothelial regions of intima.

Type II (Fatty streak lesion): As the lesion grows, it contains multiple layers of foam cells and includes lesions grossly called fatty streaks.

Type III (Preatheroma): At this stage, the lesions contain isolated pools of densely packed collection of extracellular lipids droplets (cholesterol), surrounded by foamy macrophages. These droplets disrupt the smooth intimal muscle cells.

Type IV (Atheroma): These lesions contain confluent core of extracellular lipids. This extracellular lipid is the immediate indication of a larger and more disruptive core of extracellular lipids. At this stage, a fibrous cap is formed and the penetration of plaque into the media could occur.

Type V (Fibroatheroma): At this stage, the lesion develops into a more advanced form and is characterized by a thick layer of fibrous connective tissue.

Type VI (Thrombotic lesions): This type of lesion generally has an underlying morphology of type IV or V.

2.8 Review of literature on imaging vascular plaque

There are several imaging modalities that can detect atherosclerosis. Cardiac magnetic resonance and multi-detector x-ray computed tomography are the leading non-invasive techniques that could image vulnerable plaque. Despite the advances in these non-invasive imaging methods, the option to immediately invoke treatment ensures that catheterizations will continue to be relied upon clinically to locate and then treat target lesions. Intravascular imaging will continue to play an important role for as long as interventional strategies such as balloon angioplasty, stenting and atherectomy remain front-line treatments of the disease. Intravascular ultrasound (IVUS) imaging,

introduced in the late 80s, produces circumferential tomographic images of the vessel wall. IVUS is capable of providing 3D anatomical information and is becoming increasingly used to assess plaque burden as well as guide and evaluate interventional catheterization procedures. Typical IVUS catheters operate between 20 – 40 MHz providing a 40 – 20 μm upper limit on the spatial resolution of the images. Practically, IVUS images have 2 to 5 times lower resolution compared to OCT. OCT is capable of achieving imaging resolution in the axial dimension on the 10 μm scale. The higher resolution available from IV-OCT systems is its primary advantage over the established IVUS technology Like IVUS, IV-OCT provides circumferential images of the vessel wall that enable 3D reconstruction of the vessel topography. With the higher resolution available from IV-OCT, detailed anatomical features of the vessel wall and plaque are easily visualized compared to IVUS. The argument for using IV-OCT to guide interventional procedures is compelling as the high resolution afforded by IV-OCT enables monitoring of several risk factors associated with atherosclerosis.

Optical spectroscopic techniques, such as Fluorescence, Near-Infrared (NIR) and Raman spectroscopies are the other imaging modalities used to detect plaques. Fluorescence spectroscopy allows detection of chemical composition of plaque from a examined area. It is possible to recover spatially resolved images with fluorescence, depending upon the exciting wavelength used and fiber optic excitation collection geometry. The excitation wavelength normally tends to be either in the UV range or visible range [41-43]. Advantage of fluorescence spectroscopy is that it can proficiently detect atherosclerosis. However it lacks sufficient spatial information to measure size of plaque regions.

NIR spectroscopy is another technique to detect plaque. NIR spectroscopy measures both absorption and scattering to characterize cholesterol and collagen content in plaque [44]. It can penetrate deep into tissue and thus makes it easier to differentiate between vulnerable and stable plaques [45]. The disadvantage of NIR spectroscopy is that it cannot correlate plaque thickness and lipid core depth, which is an important parameter in plaque detection [46].

Raman spectroscopy is an optical technique that yields information on biochemical composition information of tissue and can detect specific types of plaque especially calcium-laden and cholesterol-laden plaque [47]. The advantage of this technique is that the vibrational energy states are very specific to atom bonding types and thus makes it easier to identify biological compounds. However there are many disadvantages of this technique. It has a longer recording time of samples which may increase risk to patients. Also, when recording Raman signals, fluorescence emission is usually present which has to be separated from the Raman signals. Raman spectroscopy can extract information from depths exceeding few hundred micrometers [47].

Non-linear microscopy is another imaging technique that can detect atherosclerotic plaque. Non linear microscopy is based on non-linear optics. There has been studies that showed that multimodal non linear optical microscopy can provide a mean to visualize the extracellular components of plaque which can be used to determine the plaque structure [48].

2.9 Animal Model

Vascular samples of atherosclerotic plaques were harvested from myocardial infarction prone Watanabe heritable hyperlipidemic rabbits (WHHLMI) [15] (by colleagues at the Institute of Biodiagnostics, National Research Council Canada, Winnipeg). This work was approved by the local animal care committee at Institute for Biodiagnostics, National Research Council Canada. Arterial samples harvested from seven WHHLMI rabbits aged 309, 316, 330, 332, 360, 450, 480, 577, 655 and 666 days were obtained. Segments of tissue starting from the ascending aorta to the external iliac artery were excised from all specimens and subdivided into 20~30 mm long sections.

CHAPTER 3: OPTICAL COHERENCE TOMOGRAPGHY

3.1 Introduction

An optical technique which utilizes light and fiber-optics to image subsurface biological tissues is known as optical coherence tomography. Optical Coherence Tomography (OCT) is a light based imaging modality, that provides the ability to view, cross-sectional images of biological tissues with high spatial resolution. OCT is analogous to ultrasound imaging, in which sound waves are used to create images with a resolution of a few hundred microns. In Ultrasound imaging, sound waves are incident on biological tissues which could be imaged using the reflected sound waves. The resolution of the images depends on the frequency of the sound waves. The sound wave frequencies for a typical ultrasound system are approximately 10 MHz, which yield spatial resolution of approximately 150 μm. However, OCT measures the back-reflection of infrared light waves rather than sound to create images. The use of the light allows for approximately 10 times higher imaging resolution. The axial and lateral resolution of OCT is about 15 μm and 25 μm respectively, which is 10–20 times greater than standard B-mode ultrasound imaging.

Although OCT was originally developed for the field of optometry, it is currently being used in many clinical applications [49] including cardio vascular imaging [50]. OCT provides enhanced depth and clarity for viewing biological tissues compared to other medical imaging devices.

Compared to other imaging modalities, OCT has the following advantages:

(1) Time-domain and spectral-domain OCT are based on 'low-coherence interferometery', which is capable of achieving high-resolution cross-sectional images [51-53].

(2) The light source used in OCT is usually NIR, which is not harmful.

(3) The OCT system is optical fiber-based, thus can be easily made compact and low cost.

(4) OCT enables tissue to be imaged in situ and in real time [54].

Because of these and other advantages, OCT has established itself as an important tool in biomedical imaging.

3.2 OCT Operating Principles

OCT imaging systems are divided into two categories: time-domain OCT and Fourier domain OCT. Fourier Domain OCT system is further subdivided into spectral-domain OCT referred to as SD-OCT and swept source OCT termed SS-OCT. The system used in this work is a SS-OCT which is located at the Institute of Biodiagnostics, National Research Council Canada, in Winnipeg. We thus briefly review SS-OCT operating principles.

The basic set up of a SS-OCT system is shown in figure 3.1.

The narrow bandwidth frequency swept Laser light source is divided equally into sample and reference beam by an fiber optic coupler. The sample beam is incident on the tissue to be images and is back reflected from its internal structure at different depths. The reference is reflected from a fixed reference mirror at fixed delay. The sample and reference beam have a time offset determined by path length difference which is based on the depth of structure in the tissue. And therefore the light echo delay in sample beam will have frequency offset from the reference beam because the frequency sweep is a function of time, shown in below figure 3.2., (sample beam and reference as represented in difficult colors). When the reflected light from reference mirror and sample are combined the modulation in intensity is produced at a frequency is determined by this frequency offset which is proportional to path length difference. The echo delay is measured by digitizing the photo detector signal over a single frequency sweep of laser light source, and then by Fourier transforming the modulation frequency signal yields the axial scan measurement of the magnitude and echo delay of light from the tissue.

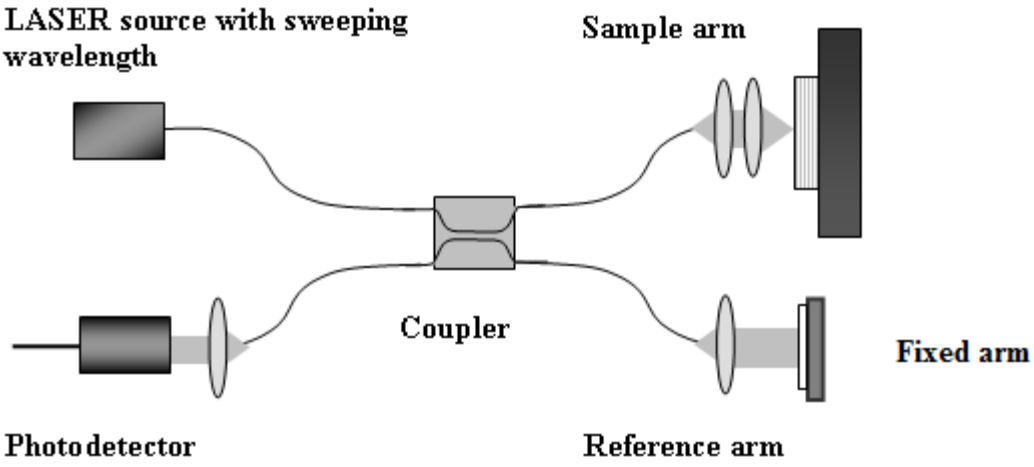

Figure 3.1 Basic configuration of a SS-OCT setup

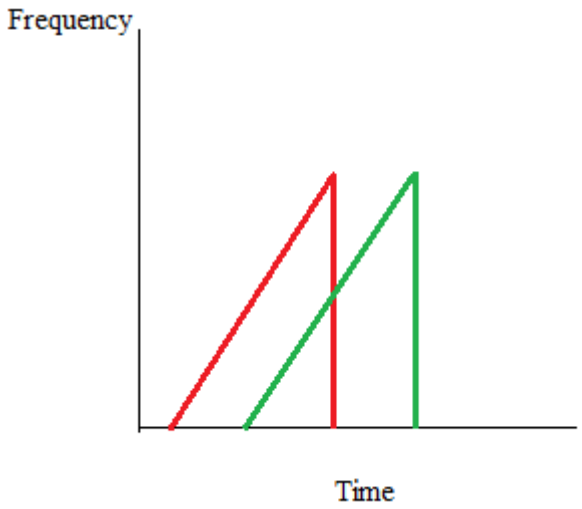

Figure 3.2 Represents frequency offset of sample beam from reference beam.

Advantages of SS-OCT [55]:

1. SS-OCT measures all the echo delay of light from the tissue at the same time unlike time domain OCT.
2. Mechanical scanning of reference path length is not required and hence there is a significant increase in imaging speed and axial scanning rate.
3. Line scan cameras are not required and therefore it has significant impact on OCT imaging of scattering tissues.

3.3 Experimental Imaging setup

The experimental setup for SS-OCT imaging was provided by Institute of Biodiagonstic, National Research Council of Canada (IBD-NRC). The wavelength-swept laser source, has a central wavelength of 1310 nm, a sweep rate of 30 kHz and a sweep range of 110nm. It provides an axial OCT resolution of about 12 μm in air. The SS-OCT unit was configured as a Mach-Zehnder interferometer with balanced optical detection.This experimental set up is shown in figure 3.3

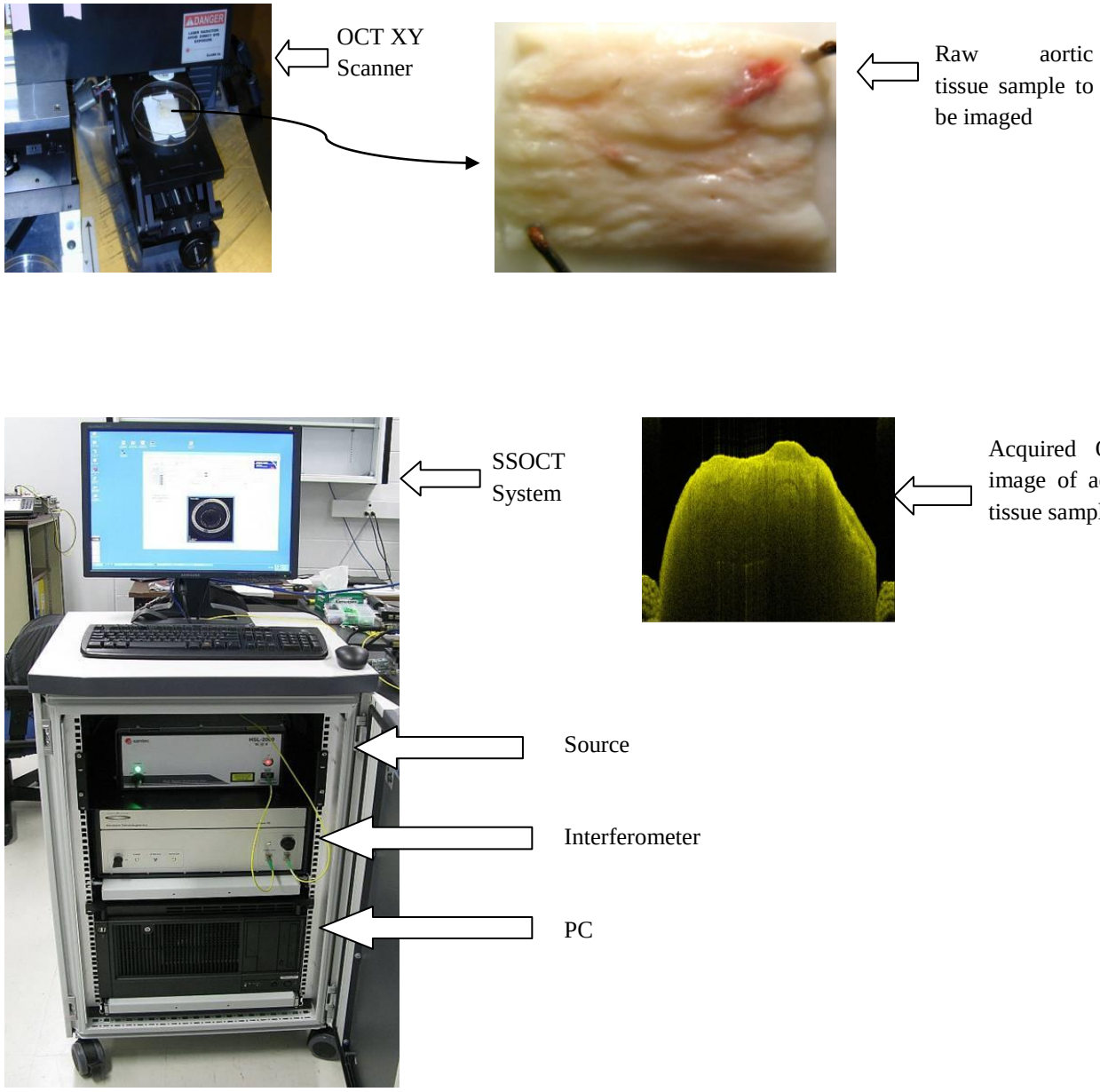

Figure 3.3 Experimental imaging set up

3.4 Application of IVOCT

OCT can be used for numerous applications. It has the potential to be used in many medical fields and applications. Heart disease and cancer and are two of the most promising areas of application. OCT imaging has the potential to improve the current cardiovascular therapies and procedures such as stenting and balloon angioplasty by providing vascular images in real time to guide stent placement and balloon inflation. OCT has the capability of visually identifying plaques in the blood stream, therefore it can differentiate between stable plaques and unstable plaques which are probably responsible for up to seventy percent of all heart attacks. In summary it could make diagnosis of artherosclerotic disease more accurate and faster. As technology becomes increasingly more advanced, it may be possible for medical physicians to perform biopsies only using optical coherence tomography imaging.

Intravascular optical coherence tomography (OCT) is a minimally invasive microscopic imaging technology that has been developed for the identification of vulnerable plaque [56-59]. Since OCT uses optical fiber probe, it is easily adaptable to coronary catheters [60] to insert into arteries and acquire the imaging of arterial pathology. The first investigation of IVOCT demonstrated its potential to perform micron-scale tomographic imaging of the internal microstructure of *in-vitro* atherosclerotic plaques [61]. Further development of OCT technology enabled intracoronary imaging in human patients [62-65].

OCT can distinguish three layers of artery wall. It demonstrates intima as signal rich layer, the media as signal poor middle layer, and adventitia as the signal rich layer [53].

With regard to tissue characterization, OCT can identify three types of vascular plaques (fibrous, fibrocalcific, and lipid-rich plaques).

Yabushita *et al.* developed the first steps in validating IVOCT imaging and testing the accuracy of objective image criteria for differentiating between components of atherosclerotic plaque. In their histology-controlled OCT study, a total 357 specimens were obtained and histopathology was used to validate the accuracy of OCT for characterizing plaque type. Validation test yielded a sensitivity and specificity ranging from 71% to 79% and 97% to 98% for fibrous plaques, 95% to 96% and 97% for fibrocalcific plaques, and 90% to 94% and 90% to 92% for lipid-rich plaques, respectively. The results from this study demonstrated that OCT is highly sensitive and specific for differentiating lipid-rich plaques from other plaque types [60].

OCT is also capable of identifying additional plaque components that may be associated with coronary events. Some of these features are described below [66].

Calcific Nodules:

Calcific nodules have been associated with plaque thrombosis in some cases [67, 68]. Studies have shown that, compared to histopathology, OCT can be used to diagnose calcific nodules with 96% sensitivity and 97% specificity [66].

Cholesterol Crystals:

Studies have shown that presence of cholesterol crystals increases the stiffness of lipids pools and thereby it may decrease the likelihood of plaque rupture [69]. OCT images of

cholesterol crystals demonstrated linear, oriented and highly reflecting structures within the plaques [70].

Giant Cells:

Giant cells (Multinucleated macrophages) are an inflammatory response to a foreign body such as cholesterol crystals within atherosclerotic plaques. Giant cells can be identified by OCT as large highly reflecting regions [66].

3.5 Comparison of IVOCT with Other Imaging Modalities

There are multiple imaging modalities that have been utilized to detect vulnerable plaques which include ultrasound (IVUS) [71-74], computed tomography [75-78], and magnetic resonance imaging [79, 80]. Several features of IVOCT that make it attractive for intra-vascular imaging are high resolution, small size of fiber-based imaging probes and availability of image processing techniques to assess OCT images to extract diagnostic information. With higher resolution available from IV-OCT, detailed anatomical features of the vessel wall and plaque are easily visualized compared to IVUS as shown in figure 3.3.

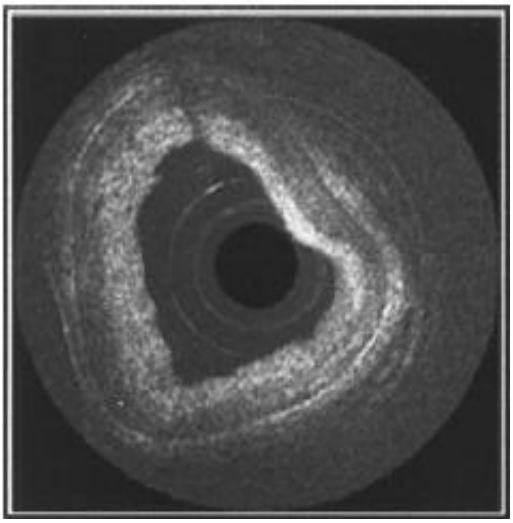

(a)

Figure 3.4 a circumferential OCT image coronary vessel

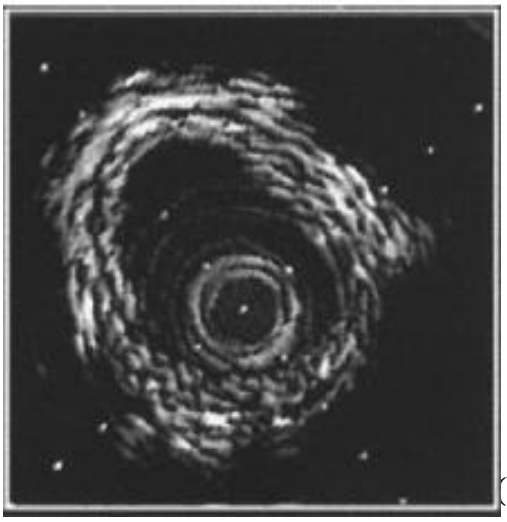

(b)

Figure 3.4.b IVUS circumferential image of a of the coronary vessel

OCT has been proven to be equivalent in detecting calcified plaque morphologies, in comparison with high resolution IVUS. Also, previous studies have shown the clinical application of OCT and its superiority to IVUS in detecting characteristics of vulnerable plaque [81]. Although IVUS is not capable of identifying microstructural features of vulnerable plaque, it can identify non-atherosclerotic vessels and arterial disruptions. A study was conducted to compare OCT-IVUS image pairs obtained from different patients [82]. In all cases it was found that IVOCT observations were more consistent than IVUS. On the basis of these findings, IVOCT has emerged as a promising imaging modality for extracting plaque diagnostic information. Studies have also shown that using texture analysis, it may be possible to differentiate between visually uniform tissue types in OCT images [83].

CHAPTER 4: SUPERVISED CLASSIFICATION OF ATHEROSCLEROSIS

Pattern recognition/classification is a broad field in machine learning that has developed to address problems such as face recognition, speech recognition, and cancer detection, etc. One major division in pattern recognition is between supervised and unsupervised classification techniques. Supervised methods require that the classifications of the samples be known and provided to the classifier. Unsupervised methods, on the other hand, do not require *a priori* knowledge of sample classifications, *i.e.*, class labels are unknown. In this chapter, we describe the texture features based design of our supervised classifier of atherosclerosis.

Our Supervised method is divided into following five sections,

1. Preprocessing of our raw OCT vascular images.

2. Extraction of statistical texture features and feature normalization.

3. Feature selection.

4. Classification using supervised learning algorithm (*Knn*).

5. Validation using *leave one out cross validation* (LOOCV).

4.1. Preprocessing of our raw OCT vascular images

Our raw OCT vascular images are represented as floating point numbers, so we performed segmentation using image normalization on each image file to achieve a uniform distribution of intensities on a standardized intensity range and to improve contrast. After image normalization, each pixel had a brightness value ranging from 0 to 255. This was performed by a Min-Max normalization operation, which preserves all relationships of the data values exactly. It would compress the normal range if extreme values or outliers exist. Min-Max normalization is carried using the following formula:

$$\text{Image} = \frac{\min(\text{Image})}{\max(\text{Image})\text{-}\min(\text{Image})} \times 255 \qquad (4.1)$$

After normalizing our image file, we performed automatic image segmentation to improve the image quality.

Examples demonstrating raw and preprocessed images are shown below:

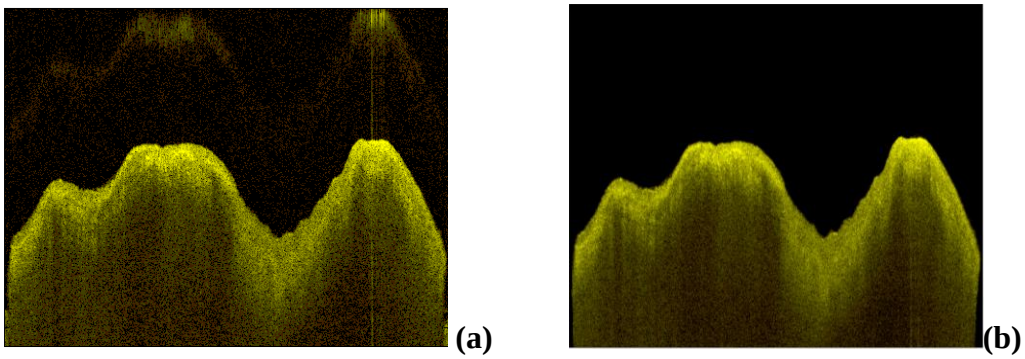

(a) **(b)**

Figure 4.1(a) Raw OCT image of vascular tissue with atherosclerotic plaque from a 11 month old WHHLML rabbit at 60th B-scan. (b) Preprocessed OCT image of vascular tissue with atherosclerotic plaque from a 11 month old WHHLML rabbit at 60th B-scan.

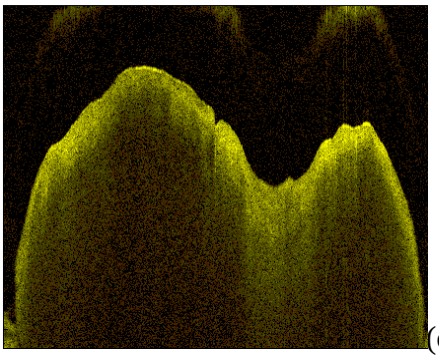
(c)
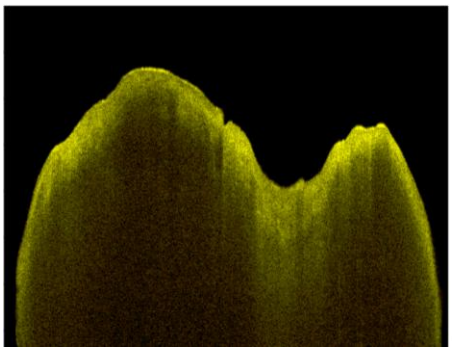
(d)

Figure 4.1(c) Raw OCT image of vascular tissue with atherosclerotic plaque from a 11 month old WHHLML rabbit at 120th B-scan. (d) Preprocessed OCT image of vascular tissue with atherosclerotic plaque from a 11 month old WHHLML rabbit at 120th B-scan.

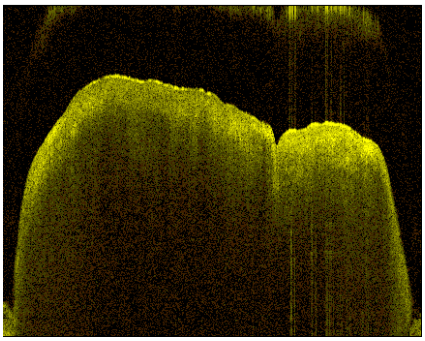
(e)
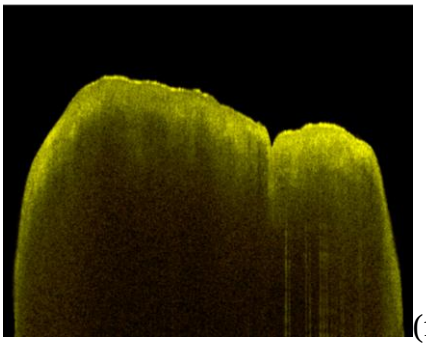
(f)

Figure 4.1(e) Raw OCT image of vascular tissue with atherosclerotic plaque from a 11 month old WHHLML rabbit at 160th B-scan. (f) Preprocessed OCT image of vascular tissue with atherosclerotic plaque from a 11 month old WHHLML rabbit at 160th B-scan.

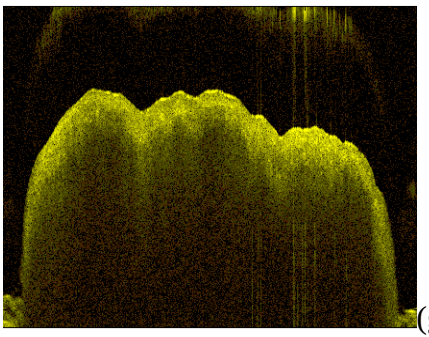
(g)
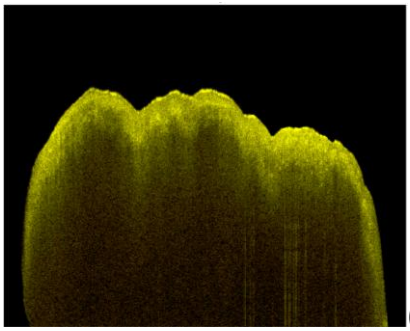
(h)

Figure 4.1(g) Raw OCT image of vascular tissue with atherosclerotic plaque from a 11 month old WHHLML rabbit at 200th B-scan. (h) Preprocessed OCT image of vascular tissue with atherosclerotic plaque from a 11 month old WHHLML rabbit at200 B-scan.

To design our supervised classifier, we used a total of 72 OCT B scan images. In supervised learning class labels has to be known. To verify the class labels we also compared the OCT images with actual photographic images of vascular tissues. We divided the images in two classes, Class A: Healthy vascular tissues. Class B: Vascular tissue with atherosclerotic plaque. We further divided these images into training and testing from each class. We used 44 training images and 28 testing images for classification. For training the classifier, we used 22 images for each class, and for testing, we used 14 images for each class.

Training Class A: 22 Healthy vascular tissues Images.

Test Class A: 14 Healthy vascular tissues Images.

Training Class B: 22 Atherosclerotic plaque Images.

Test Class B: 14 Atherosclerotic plaque Images.

4. 2 Extraction of statistical texture features and feature normalization

Definition of texture: Texture can be defined as a regular repetition of an element on a surface. Image texture is a spatial property. A single pixel in an image has no texture. Texture gives us information about the spatial arrangement of different characteristics like intensity, color, *etc.*, of an image. In medical imaging texture analysis plays an important role in the characterization of tissues. Texture analysis in medical imaging is an ongoing field of research, with applications ranging from the segmentation of specific tissue structures, detection of lesions and differentiation between healthy and unhealthy tissues.

4.2.1 Feature extraction:

We extracted texture features on our processed OCT vascular images using the SGLDM method, which is a known method for extracting second order statistical texture features. Features derived from the SGLDM method have been widely used for classification of tissue images [83-86]. Rosenfeld and Troy [87] and Haralick *et al.* [88] first proposed SGLDM matrices for arbitrary spatial distances and angular directions. The two parameters used to construct SGLDM matrices are 1. Relative distance among image pixels, d and 2. Relative orientation among pixels $\boldsymbol{\theta}$.

The SGLDM method determines the probability of occurrence of grey levels with respect to relative spatial pixel positions in an image. The SGLDM matrices are based on an estimate of second-order joint conditional probability density functions p (i, j: d, θ) [89-92]. These probability density functions, p (i, j: d, θ), measure the probability that

two pixels, which are located with an inter sample distance, d and direction, θ, have gray levels i and j. To detect the atherosclerotic plaque using these SGLDMs, we extracted 11 texture features in two directions as shown in figure 4.1 with d=1.

Even though these textural features contain information about textural characteristics of an image, it is difficult to identify which specific textural characteristic is represented by each of these features [88]. However few of the features have visual definition like F1 (Angular second moment) is the measure of smoothness of the image. The less smooth the region is , the lower the ASM.

F2 (Contrast), is a measure of local gray level variations of pixels in an image.

F4(Inverse difference moment) as defined in table 4.1, takes high value for low contrast images since it has the i-j (local gray level variation) in the denominator.

F8 (Entropy), is the measure of randomness in an image. For smooth images, the value of entropy will be low.

Other features represent the nature of gray level transition within the image.

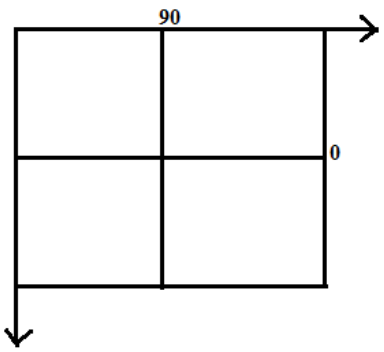

Figure 4.2 The two orientations we used to construct SGLDM matrices.

Example to construct SGLDM matrices:

Let I (i,j) be an 4 ×4 image .

$$\boldsymbol{I} = \begin{bmatrix} 1 & 2 & 1 & 2 \\ 1 & 2 & 0 & 1 \\ 1 & 0 & 2 & 1 \\ 1 & 2 & 2 & 1 \end{bmatrix} \qquad (4.2)$$

A 4×4 image with three grey levels N_g= 0, 1, and 2

$$A = \frac{1}{R}\begin{bmatrix} \eta(0,0) & \eta(0,1) & \eta(0,2) \\ \eta(1,0) & \eta(1,1) & \eta(1,2) \\ \eta(2,0) & \eta(2,1) & \eta(2,2) \end{bmatrix}$$

The SGLDM matrix for a pair (d, $\boldsymbol{\theta}$), R is the total number of pixel pairs

$$A^0(d=1) = \frac{1}{23}\begin{bmatrix} 0 & 3 & 2 \\ 2 & 0 & 6 \\ 2 & 6 & 2 \end{bmatrix}\begin{matrix} 0 \\ 1 \\ 2 \end{matrix}$$
$$\begin{matrix} 0 & 1 & 2 \end{matrix}$$

The SGLDM matrix for image in 4.2 with d = 1, $\boldsymbol{\theta}$=0

For each of the intensity pairs, such as (0, 0), we count the number of pixel pairs at relative distance d =1 and orientation $\boldsymbol{\theta}$=0◦ that take these values.

We calculated the following features from SGLDM matrices :

Table 4.1 SGLDM features and their mathematical expressions.

Feature Number	Feature name	Formula
F1	Angular Second Moment(0)	$\sum_i \sum_j (P(i,j)^2)$
F2	Contrast(0)	$\sum_{n=0}^{N_g-1} n^2 \left\{ \sum_i \sum_{\substack{j \\ \lvert i-j \rvert = n}} P(i,j) \right\}$
F3	Variance(0)	$\sum_i \sum_j (i-\mu)^2 P(i,j)$
F4	Inverse Difference Moment(0)	$\sum_i \sum_j \frac{P(i,j)}{1+(i-j)^2}$
F5	Sum(difference) Average(0)	$\sum_{i=0}^{2(N_g-1)} iP_{x+(-)y}(i)$
F6	Sum Variance(0)	$\sum_{i=0}^{2N_g-2} (i-F_5)^2 P_{x+y}(i)$
F7	Sum Entropy(0)	$-\sum_{i=0}^{2Ng-2} P_{x+y}(i) \log\{P_{x+y}(i)\}$
F8	Entropy(0)	$-\sum_i \sum_j P(i,j) \log P(i,j)$
F9	Difference Variance(0)	$-\sum_{i=0}^{Ng-1} (i-F_5)^2 P_{x-y}(i)$
F10	Difference Entropy(0)	$-\sum_{i=0}^{Ng-1} P_{x-y}(i) \log P_{x-y}(i)$
F11	Information Measure II of correlation(0)	$\sqrt{1-\exp(-2(H_{xy}^2 - H_{xy}))}$ Where, $H_{xy}^2 = -\sum_j \sum_i P_x(i) P_y(j) \log(P_x(i) P_y(j))$
F12	Angular Second Moment(90)	$\sum_i \sum_j (P(i,j)^2)$
F13	Contrast(90)	$\sum_{n=0}^{N_g-1} n^2 \left\{ \sum_i \sum_{\substack{j \\ \lvert i-j \rvert = n}} P(i,j) \right\}$

F14	Variance(90)	$\sum_i \sum_j (i-\mu)^2 P(i,j)$
F15	Inverse Difference Moment(90)	$\sum_i \sum_j \frac{P(i,j)}{1+(i-j)^2}$
F16	Sum(difference) Average(90)	$\sum_{i=0}^{2(N_g-1)} iP_{x+(-)y}(i)$
F17	Sum Variance(90)	$\sum_{i=0}^{2N_g-2} (i-F_{16})^2 P_{x+y}(i)$
F18	Sum Entropy(90)	$-\sum_{i=0}^{2Ng-2} P_{x+y(i)} \log\{P_{x+y}(i)\}$
F19	Entropy(90)	$-\sum_i \sum_j P(i,j) \log P(i,j)$
F20	Difference Variance(90)	$-\sum_{i=0}^{Ng-1} (i-F_{16})^2 P_{x-y}(i)$
F21	Difference Entropy(90)	$-\sum_{i=0}^{Ng-1} P_{x-y}(i) \log P_{x-y}(i)$
F22	Information Measure II of correlation(90)	$\sqrt{1-\exp(-2(H_{xy}^2 - H_{xy}))}$ Where, $H_{xy}^2 = -\sum_j \sum_i P_x(i) P_y(j) \log(P_x(i) P_y(j))$

Where,

P(i, j) , $(i, j)^{th}$ entry in SGLDM matrix, = P(i, j)/R.

$P_x(i)$, the marginal probability of ith entry = $\sum_{j=1}^{N_g} P(i,j)$.

N_g is the number of gray levels in the images

$P_y(i)$, the marginal probability of jth entry = $\sum_{j=1}^{N_g} P(i,j)$

4.2.2 Feature normalization

The scale of the features lied within a different dynamic range. We normalized the entire 22 feature vector. Feature normalization ensures that all the features have same influence on performance of the classifier. Each feature vector of an image is normalized as follows:

$$\hat{x} = \frac{x - \bar{x}}{\sigma} \tag{4.3}$$

Where, $\hat{x}$ is the normalized value , x is the raw feature vector , $\bar{x}$ is the sample mean and σ is the standard deviation.

4.3. Feature selection

We generated 22 features, out of which some may be not very informative or may have high mutual correlation. Also, to achieve good generalization performance of the classifier, the dimension of the feature space must be relatively small with respect to the number of training points. In this study, we reduced the dimension of feature space by a feature selection procedure. It is a method that selects the most informative features so as to reduce their number and retain class discriminatory information. Our feature selection consists of three steps,

1. Scalar feature selection suing Fisher's Discriminant ratio (FDR) as a class separability criterion and also finding the cross correlation between the pairs of features and ranking them.
2. Finally we employed exhaustive search method to find the top 5 features.

After the feature normalization procedure, features were ranked in descending order using FDR criterion by considering each feature independently. FDR [93] was calculated using the following equation

$$FDR = \frac{(\mu_1 - \mu_2)^2}{\sigma_1^2 + \sigma_2^2} \quad (4.4)$$

Where, μ_1 and μ_2 are mean values of each feature of all the data point from both the classes and σ_1^2 and σ_2^2 are the variances of each feature from the two classes.

Table 4.2. Fisher discriminant ratio of all 22 features.

Feature Number	FDR value	Feature Rank
F2	1.859	1
F9	1.834	2
F12	1.06	3
F1	0.985	4
F6	0.915	5
F20	0.851	6
F13	0.823	7
F17	0.784	8
F15	0.772	9
F8	0.56	10
F5	0.536	11
F14	0.513	12
F18	0.476	13
F7	0.469	14
F16	0.452	15
F3	0.37	16

F19	0.341	17
F21	0.249	18
F11	0.145	19
F10	0.109	20
F22	0.096	21
F4	0.08	22

Scalar features selection process considers each feature independently and doesn't take into account the existing correlation between feature pairs. Finding the cross correlation between the feature pairs, will result in further effective feature selection process. The formula for finding the cross correlation between feature pairs are given as follows:

$$\rho_{ij} = \frac{\sum_{n=1}^{N} x_{n,i} x_{n,j}}{\sqrt{\sum_{n=1}^{N} x^2_{n,i} \sum_{n=1}^{N} x^2_{n,j}}} \qquad (4.5)$$

Where i and j are the index of the feature number, $i \neq j$,

N= number of classes, (N=2)

We again ranked the features according to their cross correlation and selected the top 16 features out 22

Table 4.3. Feature ranking of top 16 features

Feature rank	Feature number
1	**F2**
2	**F9**
3	**F6**
4	**F5**
5	**F8**
6	**F10**
7	**F4**

8	**F3**
9	**F7**
10	**F1**
11	**F15**
12	**F14**
13	**F18**
14	**F21**
15	**F12**
16	**F19**

From all 22 features, we selected 16 top ranked features and applied exhaustive search method to select the final combination of 5 best features.

Exhaustive search method, is the technique in which all possible combinations of features will be exhaustively formed. And for each combination of features, the class separability measured is calculated. We used the following measure as class separability criterion for exhaustive search method

The class separability criterion, J [*9*4] used in exhaustive search method is as follows

$$J = \text{Trace}(S_w^{-1} S_m) \tag{4.6}$$

Where, S_m is mixture scatter matrix,

$$S_m = S_w + S_b \tag{4.7}$$

Where S_w is within class scatter matrix, S_b is between class scatter matrix.

The combination of our final 5 best features is F2, F4, F6, F9 and F10.

4.4 Image classification Algorithm

We employed a non parametric image classification program in the selected feature space to classify atherosclerotic plaque in young and old WHHML rabbits. In this work we used K nearest neighbor classifier (K-nn) with K=5. The K-nn classifier is based on non-parametric density estimation techniques. The Knn classifier decides the class label of an object by analyzing its k nearest neighbors within the training points [95].

Example of K-nn with K=3 and K=5 is shown in figure 4.1.

When K=3, the test data point (black circle) is assigned to green square class because there are two squares inside the inner circle.

When K= 5, the test data point (black circle) is assigned to red cross class because the majority of points inside the outer circle are red cross.

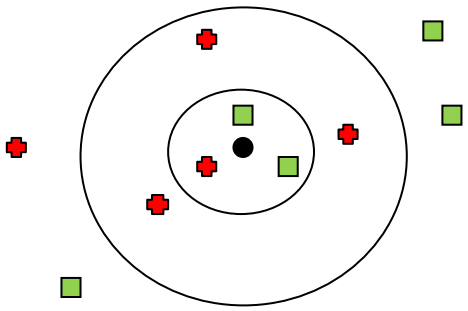

Figure 4.3. Example of K nn with K=3 and K=5

Given an unknown sample, the K-nn classifier identifies 5 nearest neighbors using Euclidean distance measure, regardless of the class label. Out of these 5 nearest neighbor samples, it identifies the number of samples that belong to the class A (Healthy vascular tissues Images.) and class B (Atherosclerotic plaque Images). An unknown sample is classified to either of the classes with the maximum of nearest neighbors' vote. According to the K-nn rule, each unlabeled sample is classified by the majority vote of its nearest neighbors in the training set. This rule is independent of underlying joint distribution on the sample points and their classifications [96].

4.5 Validation

To evaluate our classifier's performance we applied *leave one out cross validation* (LOOCV) method. The total number of dataset available was limited; LOOCV is very useful when there's only limited dataset available [97]. In this method one sample from the dataset is set aside, and the classification model is built on the remaining N-1 samples. The left out sample is then classified by this new model. This procedure is repeated N times, and each time a different sample is set aside as shown in Figure 4.3.

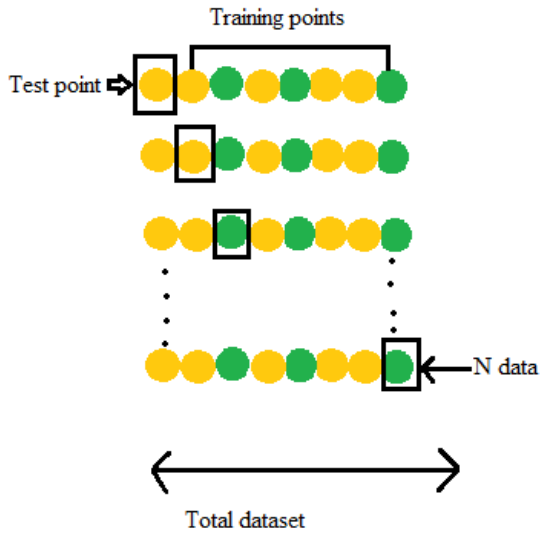

Figure 4.4. Schematic illustration of the data partitioning for leave one out cross-validation

Of our 58 training samples, 57 samples were used for training the classifier and the validation was carried out using the excluded samples. This same procedure was repeated 58 times, each time leaving out a different sample. For each misclassification an error was counted. We obtained LOOCV error as 4.54%.

Classification Error	**10.71%**
Validation Error	4.54%

Following are the images used for training and testing purpose.

Training Images of class B (22 images)

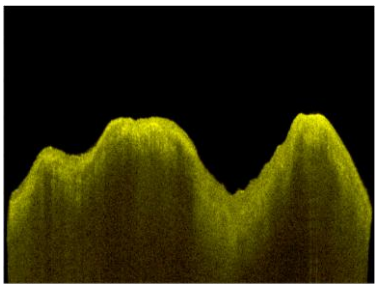
(1)

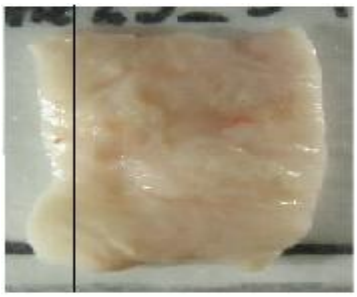

Figure 4.5.1. Preprocessed OCT image of vascular tissue with atherosclerotic plaque from a 11 month old WHHLML rabbit at 60th B-scan. Figure4.5.2. Photographic image of vascular tissue with atherosclerotic from a 11 month old WHHLML rabbit.

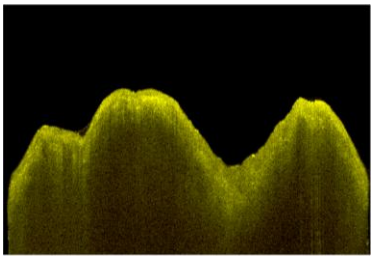
(3)

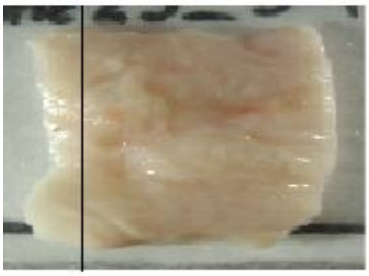
(4)

Figure 4.5.3. Preprocessed OCT image of vascular tissue with atherosclerotic plaque from a 11 month old WHHLML rabbit at 70th B-scan. Figure4.5.4. Photographic image of vascular tissue with atherosclerotic from a 11 month old WHHLML rabbit.

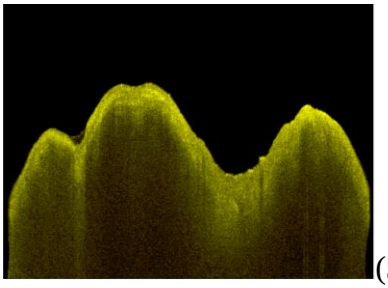
(5)

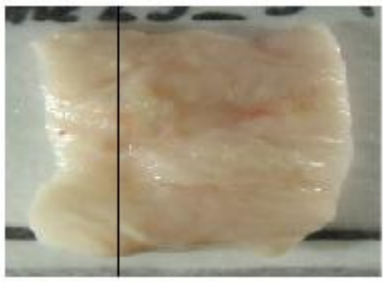
(6)

Figure 4.5.5. Preprocessed OCT image of vascular tissue with atherosclerotic plaque from a 11 month old WHHLML rabbit at 80th B-scan. Figure4.5.6. Photographic image of vascular tissue with atherosclerotic from a 11 month old WHHLML rabbit.

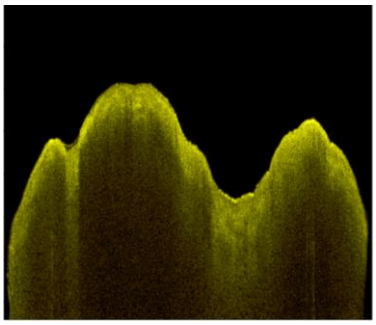

(7)

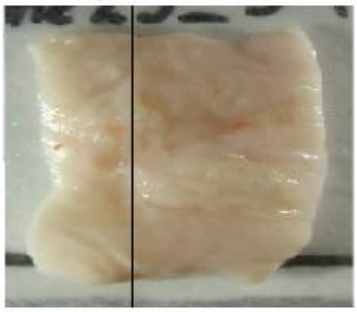

(8)

Figure 4.5.7. Preprocessed OCT image of vascular tissue with atherosclerotic plaque from a 11 month old WHHLML rabbit at 90th B-scan. Figure4.5.8. Photographic image of vascular tissue with atherosclerotic from a 11 month old WHHLML rabbit.

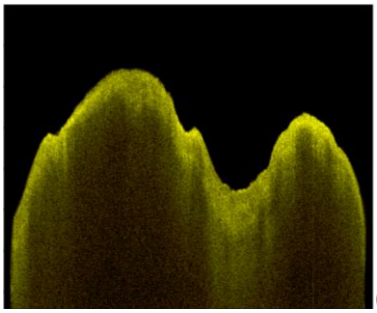

(9)

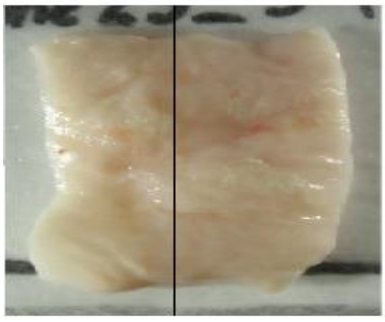

(10)

Figure 4.5.9. Preprocessed OCT image of vascular tissue with atherosclerotic plaque from a 11 month old WHHLML rabbit at 100th B-scan. Figure4.5.10. Photographic image of vascular tissue with atherosclerotic from a 11 month old WHHLML rabbit.

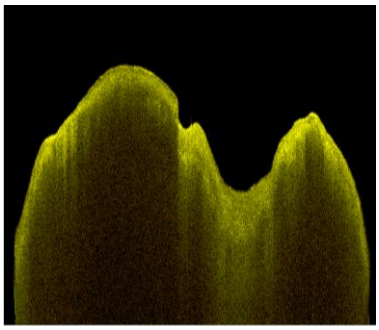

(11)

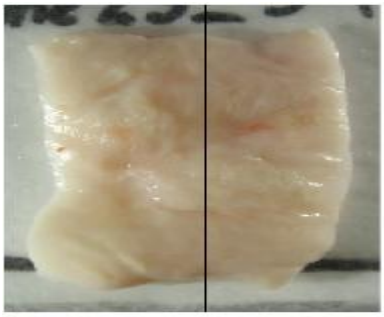

(12)

Figure 4.5.11. Preprocessed OCT image of vascular tissue with atherosclerotic plaque from a 11 month old WHHLML rabbit at 110th B-scan. Figure4.5.12. Photographic image of vascular tissue with atherosclerotic from a 11 month old WHHLML rabbit.

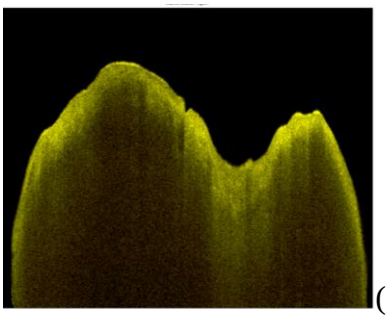

(13)

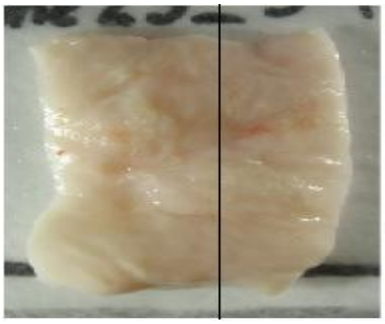

(14)

Figure 4.5.13. Preprocessed OCT image of vascular tissue with atherosclerotic plaque from a 11 month old WHHLML rabbit at 120th B-scan. Figure 4.5.14. Photographic image of vascular tissue with atherosclerotic from a 11 month old WHHLML rabbit.

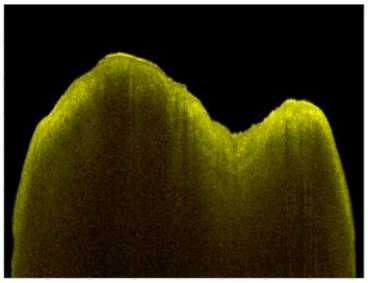

(15)

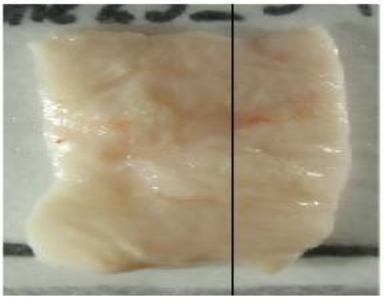

(16)

Figure 4.5.15. Preprocessed OCT image of vascular tissue with atherosclerotic plaque from a 11 month old WHHLML rabbit at 130th B-scan. Figure 4.5.16. Photographic image of vascular tissue with atherosclerotic from a 11 month old WHHLML rabbit.

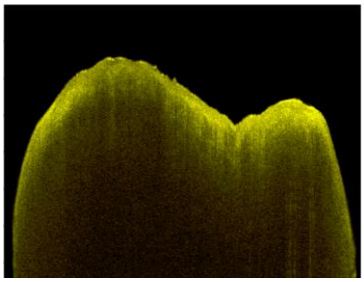

(17)

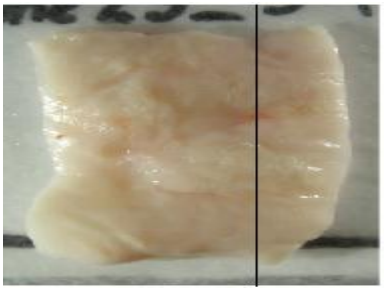

(18)

Figure 4.5.17. Preprocessed OCT image of vascular tissue with atherosclerotic plaque from a 11 month old WHHLML rabbit at 140th B-scan. Figure4.5.18. Photographic image of vascular tissue with atherosclerotic from a 11 month old WHHLML rabbit.

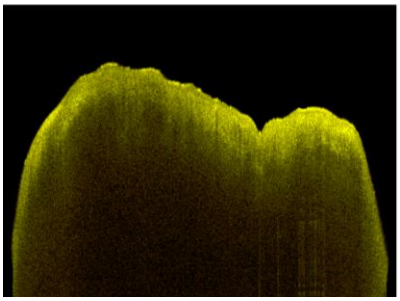

(19)

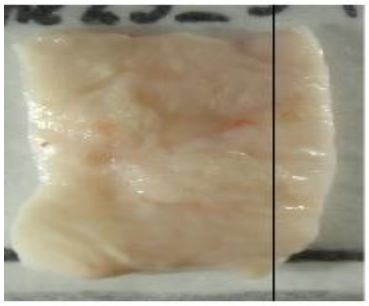

(20)

Figure 4.5.19. Preprocessed OCT image of vascular tissue with atherosclerotic plaque from a 11 month old WHHLML rabbit at 150th B-scan. Figure4.5.20. Photographic image of vascular tissue with atherosclerotic from a 11 month old WHHLML rabbit.

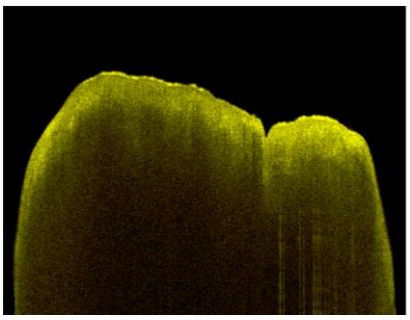

(21)

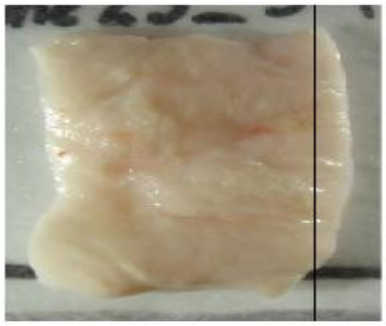

(22)

Figure 4.5.21. Preprocessed OCT image of vascular tissue with atherosclerotic plaque from a 11 month old WHHLML rabbit at 160th B-scan. Figure4.5.22. Photographic image of vascular tissue with atherosclerotic from a 11 month old WHHLML rabbit.

Testing images of class B(14 Images)

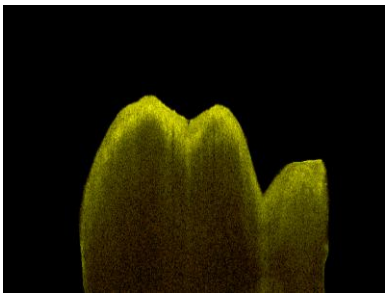
(1)

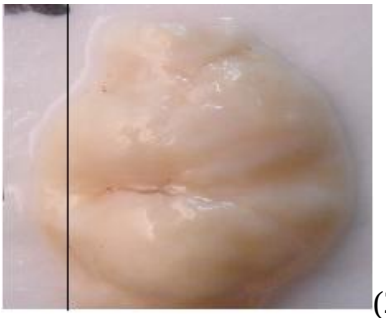
(2)

Figure 4.6.1. Preprocessed OCT image of vascular tissue with atherosclerotic plaque from a 10 month old WHHLML rabbit at 60th B-scan. Figure4.6.2. Photographic image of vascular tissue with atherosclerotic from a 10 month old WHHLML rabbit.

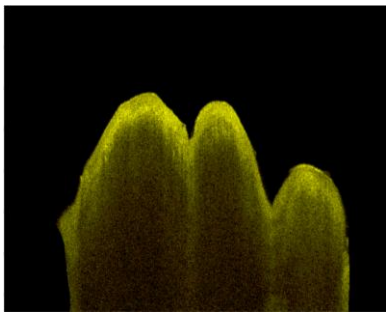
(3)


(4)

Figure 4.6.3. Preprocessed OCT image of vascular tissue with atherosclerotic plaque from a 10 month old WHHLML rabbit at 70th B-scan. Figure4.6.4. Photographic image of vascular tissue with atherosclerotic from a 10 month old WHHLML rabbit.

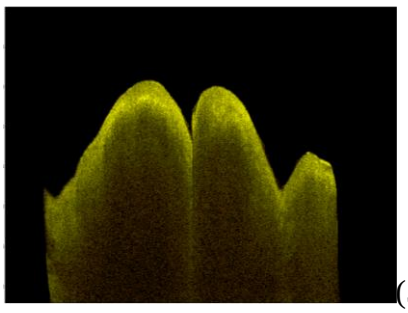
(5)

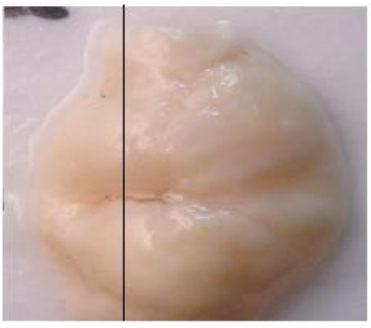
(6)

Figure 4.6.5. Preprocessed OCT image of vascular tissue with atherosclerotic plaque from a 10 month old WHHLML rabbit at 80th B-scan. Figure4.6.6. Photographic image of vascular tissue with atherosclerotic from a 10 month old WHHLML rabbit.

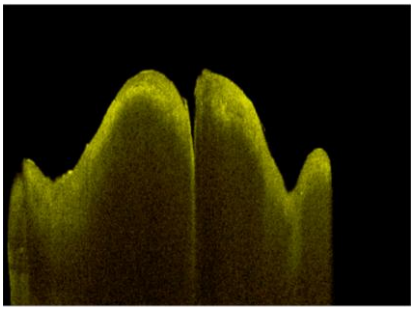

(7)

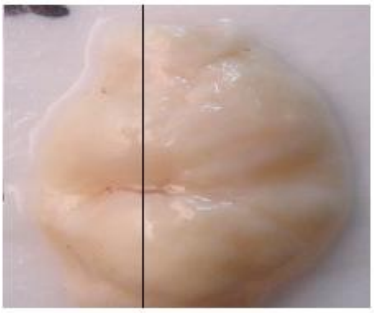

(8)

Figure 4.6.7. Preprocessed OCT image of vascular tissue with atherosclerotic plaque from a 10 month old WHHLML rabbit at 90th B-scan. Figure4.6.8. Photographic image of vascular tissue with atherosclerotic from a 10 month old WHHLML rabbit.

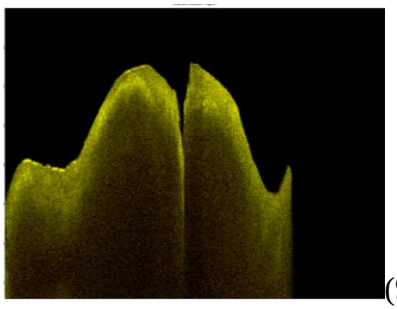

(9)

(10)

Figure 4.6.9. Preprocessed OCT image of vascular tissue with atherosclerotic plaque from a 10 month old WHHLML rabbit at 100th B-scan. Figure 4.6.10. Photographic image of vascular tissue with atherosclerotic from a 10 month old WHHLML rabbit.

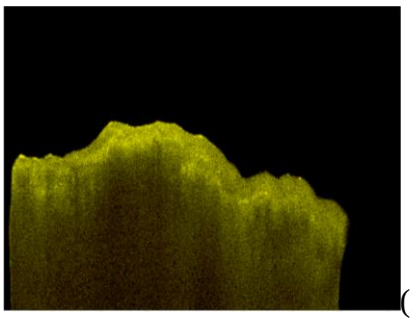

(11)

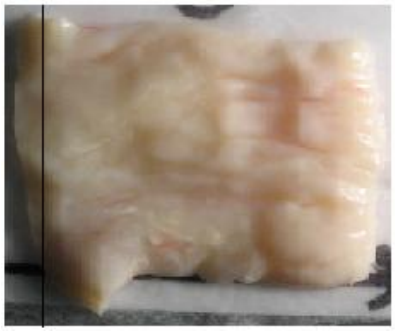

(12)

Figure 4.6.11. Preprocessed OCT image of vascular tissue with atherosclerotic plaque from a 10 month old WHHLML rabbit at 60th B-scan. Figure4.6.12. Photographic image of vascular tissue with atherosclerotic from a 10 month old WHHLML rabbit.

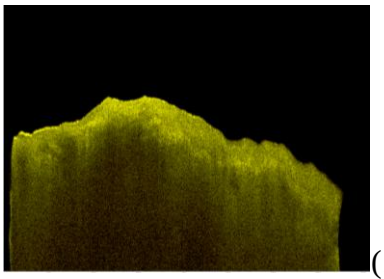
(13)

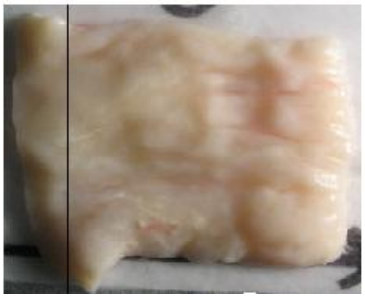
(14)

Figure 4.6.13. Preprocessed OCT image of vascular tissue with atherosclerotic plaque from a 10 month old WHHLML rabbit at 70th B-scan. Figure4.6.14. Photographic image of vascular tissue with atherosclerotic from a 10 month old WHHLML rabbit.

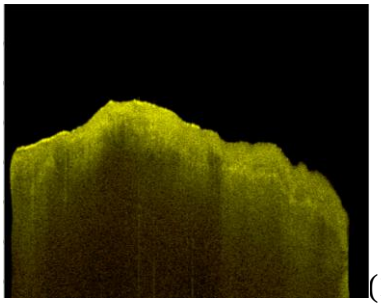
(15)

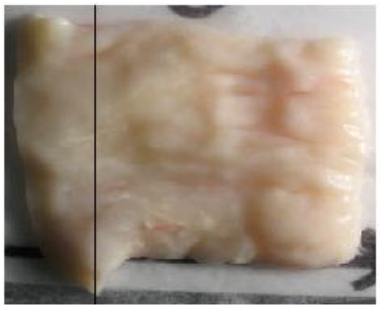
(16)

Figure 4.6.15. Preprocessed OCT image of vascular tissue with atherosclerotic plaque from a 10 month old WHHLML rabbit at 80th B-scan. Figure4.6.16. Photographic image of vascular tissue with atherosclerotic from a 10 month old WHHLML rabbit.

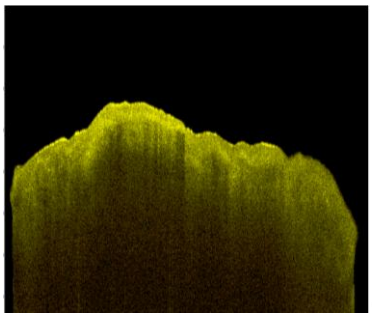
(17)


(18)

Figure 4.6.17. Preprocessed OCT image of vascular tissue with atherosclerotic plaque from a 10 month old WHHLML rabbit at 90th B-scan. Figure4.6.18. Photographic image of vascular tissue with atherosclerotic from a 10 month old WHHLML rabbit.

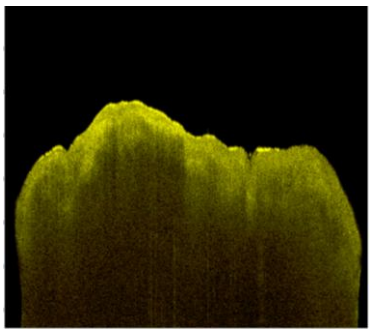

(19)

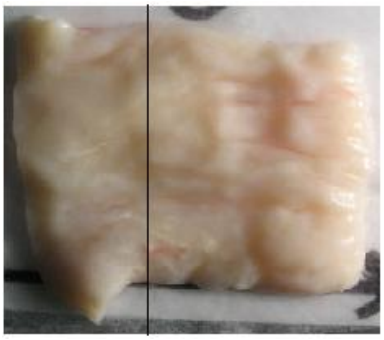

(20)

Figure 4.6.19. Preprocessed OCT image of vascular tissue with atherosclerotic plaque from a 10 month old WHHLML rabbit at 100th B-scan. Figure4.6.20. Photographic image of vascular tissue with atherosclerotic from a 10 month old WHHLML rabbit.

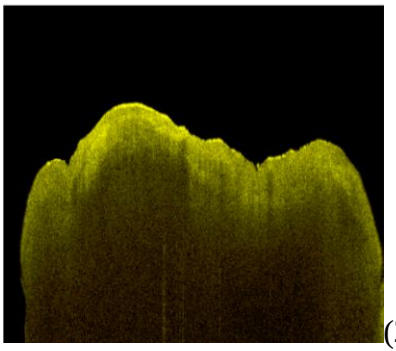

(21)

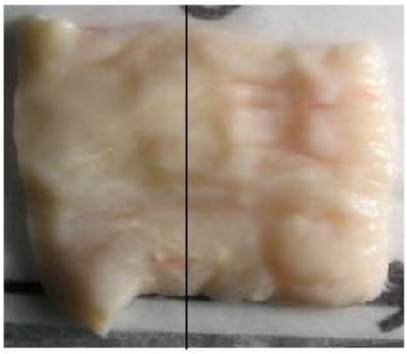

(22)

Figure 4.6.21. Preprocessed OCT image of vascular tissue with atherosclerotic plaque from a 10 month old WHHLML rabbit at 110th B-scan. Figure4.6.22. Photographic image of vascular tissue with atherosclerotic from a 10 month old WHHLML rabbit.

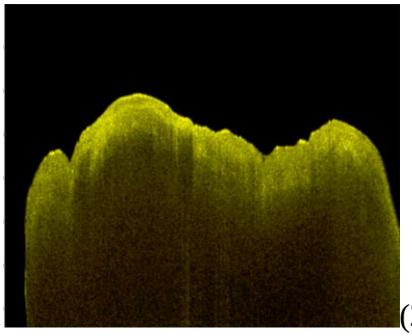

(23)

(24)

Figure 4.6.23. Preprocessed OCT image of vascular tissue with atherosclerotic plaque from a 10 month old WHHLML rabbit at 120th B-scan. Figure4.6.24. Photographic image of vascular tissue with atherosclerotic from a 10 month old WHHLML rabbit.

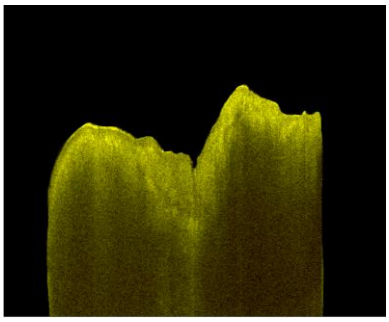

(25)

(26)

Figure 4.6.25. Preprocessed OCT image of vascular tissue with atherosclerotic plaque from a 22 month old WHHLML rabbit at 60th B-scan. Figure4.6.26. Photographic image of vascular tissue with atherosclerotic from a 22 month old WHHLML rabbit.

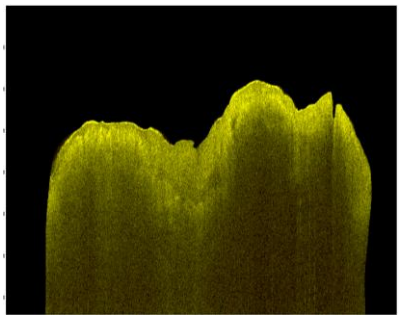

(27)

(28)

Figure 4.6.27. Preprocessed OCT image of vascular tissue with atherosclerotic plaque from a 22 month old WHHLML rabbit at 70th B-scan. Figure 4.6.28. Photographic image of vascular tissue with atherosclerotic from a 22 month old WHHLML rabbit.

Training Images of class A (22 Images)

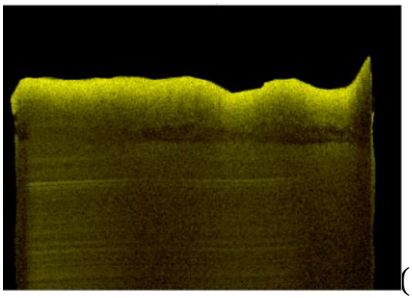
(1)


(2)

Figure 4.7.1. Preprocessed OCT image of vascular tissue with atherosclerotic plaque from a 4 month old WHHLML rabbit at 150th B-scan. Figure 4.7.2. Photographic image of vascular tissue with atherosclerotic from a 4 month old WHHLML rabbit.

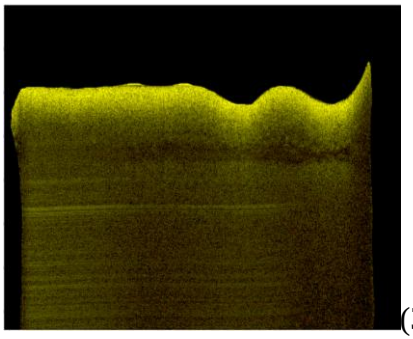
(3)


(4)

Figure 4.7.3. Preprocessed OCT image of vascular tissue with atherosclerotic plaque from a 4 month old WHHLML rabbit at 160th B-scan. Figure 4.7.4. Photographic image of vascular tissue with atherosclerotic from a 4 month old WHHLML rabbit.

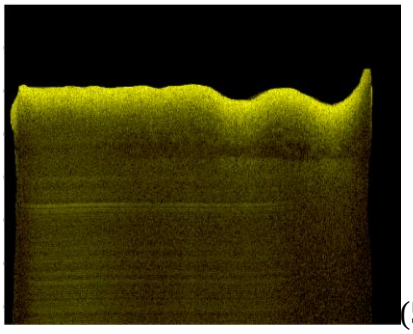
(5)


(6)

Figure 4.7.5. Preprocessed OCT image of vascular tissue with atherosclerotic plaque from a 4 month old WHHLML rabbit at 170th B-scan. Figure 4.7.6. Photographic image of vascular tissue with atherosclerotic from a 4 month old WHHLML rabbit.

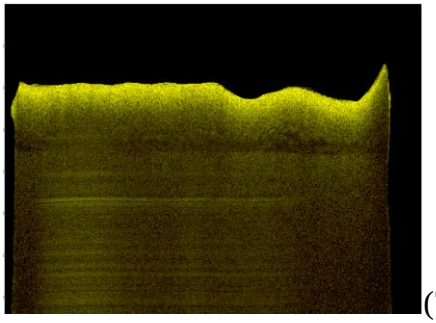

(7)

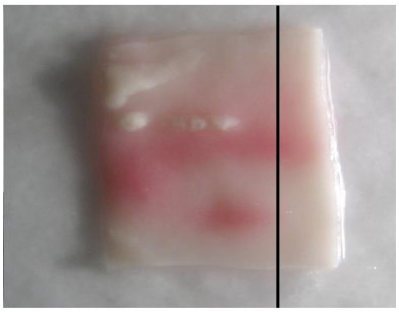

(8)

Figure 4.7.7. Preprocessed OCT image of vascular tissue with atherosclerotic plaque from a 4 month old WHHLML rabbit at 180th B-scan. Figure 4.7.8. Photographic image of vascular tissue with atherosclerotic from a 4 month old WHHLML rabbit.

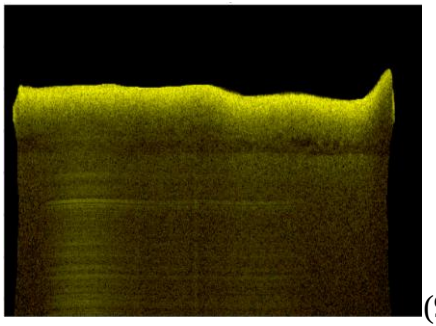

(9)

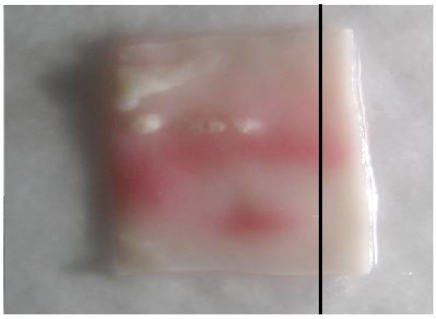

(10)

Figure 4.7.9. Preprocessed OCT image of vascular tissue with atherosclerotic plaque from a 4 month old WHHLML rabbit at 190th B-scan. Figure 4.7.10. Photographic image of vascular tissue with atherosclerotic from a 4 month old WHHLML rabbit.

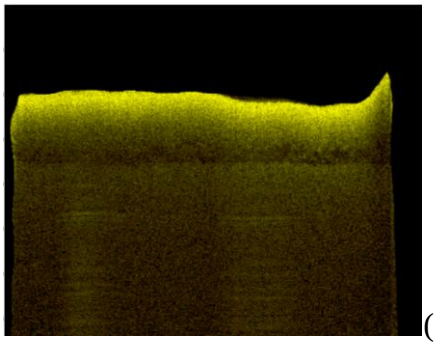

(11)

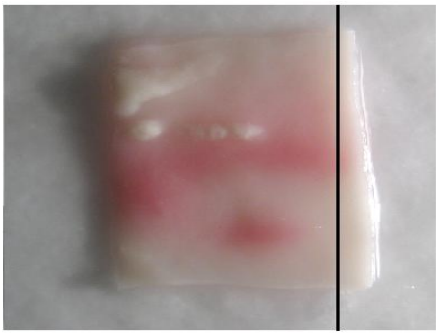

(12)

Figure 4.7.11. Preprocessed OCT image of vascular tissue with atherosclerotic plaque from a 4 month old WHHLML rabbit at 200th B-scan. Figure 4.7.12. Photographic image of vascular tissue with atherosclerotic from a 4 month old WHHLML rabbit.

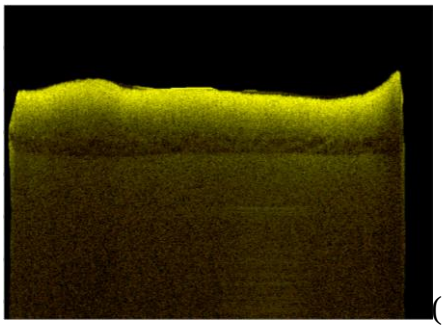

(13)

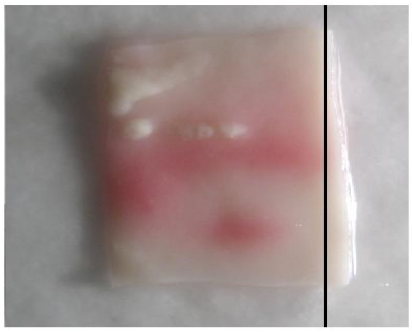

(14)

Figure 4.7.13. Preprocessed OCT image of vascular tissue with atherosclerotic plaque from a 4 month old WHHLML rabbit at 210th B-scan. Figure 4.7.14. Photographic image of vascular tissue with atherosclerotic from a 4 month old WHHLML rabbit.

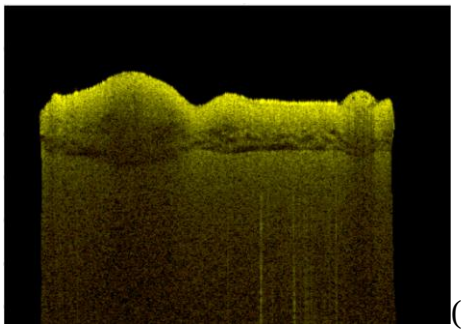

(15)

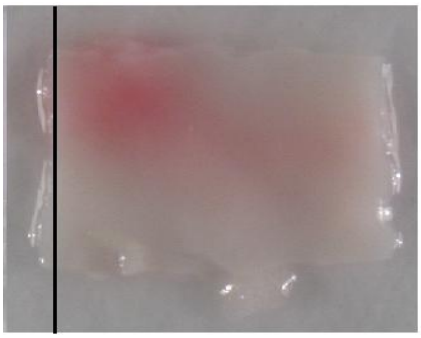

(16)

Figure 4.7.15. Preprocessed OCT image of vascular tissue with atherosclerotic plaque from a 4 month old WHHLML rabbit at 60th B-scan. Figure 4.7.16. Photographic image of vascular tissue with atherosclerotic from a 4 month old WHHLML rabbit.

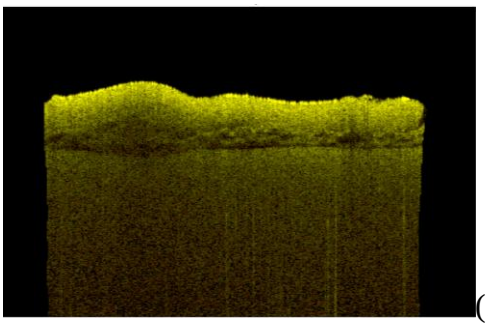

(17)

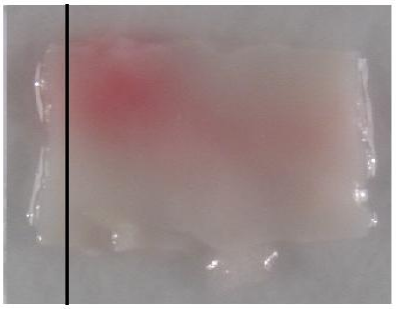

(18)

Figure 4.7.17. Preprocessed OCT image of vascular tissue with atherosclerotic plaque from a 4 month old WHHLML rabbit at 70th B-scan. Figure 4.7.18. Photographic image of vascular tissue with atherosclerotic from a 4 month old WHHLML rabbit.

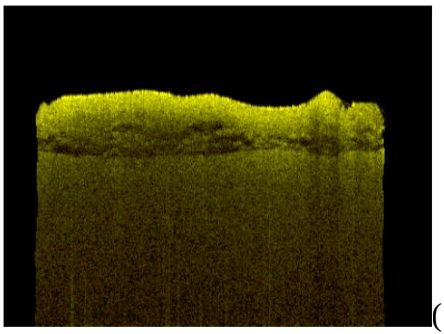

(19)

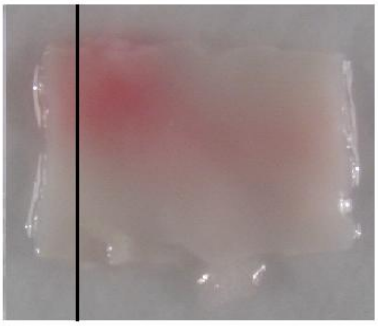

(20)

Figure 4.7.19. Preprocessed OCT image of vascular tissue with atherosclerotic plaque from a 4 month old WHHLML rabbit at 80th B-scan. Figure 4.7.20. Photographic image of vascular tissue with atherosclerotic from a 4 month old WHHLML rabbit.

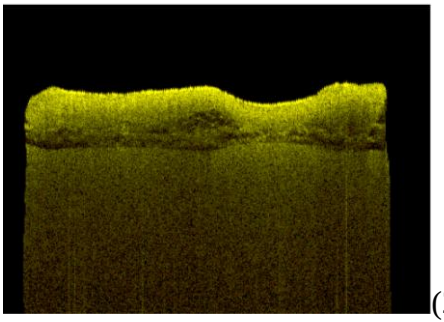

(21)

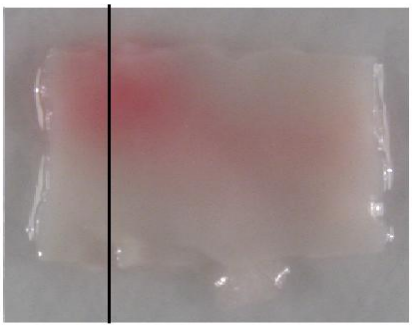

(22)

Figure 4.7.21. Preprocessed OCT image of vascular tissue with atherosclerotic plaque from a 4 month old WHHLML rabbit at 90th B-scan. Figure 4.7.22. Photographic image of vascular tissue with atherosclerotic from a 4 month old WHHLML rabbit.

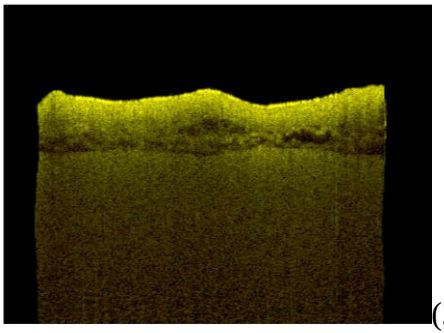

(23)

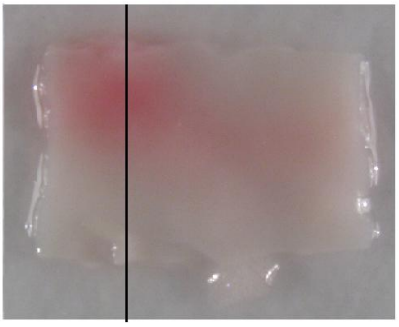

(24)

Figure 4.7.23. Preprocessed OCT image of vascular tissue with atherosclerotic plaque from a 4 month old WHHLML rabbit at 100th B-scan. Figure 4.7.14. Photographic image of vascular tissue with atherosclerotic from a 4 month old WHHLML rabbit.

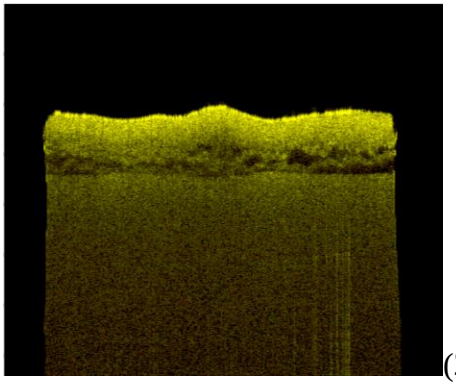

(25)

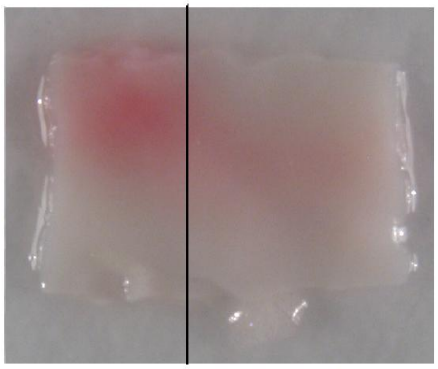

(26)

Figure 4.7.25. Preprocessed OCT image of vascular tissue with atherosclerotic plaque from a 4 month old WHHLML rabbit at 110th B-scan. Figure 4.7.26. Photographic image of vascular tissue with atherosclerotic from a 4 month old WHHLML rabbit.

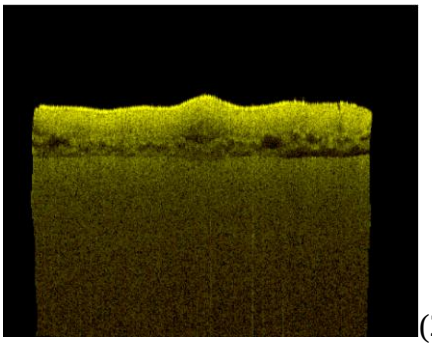

(27)

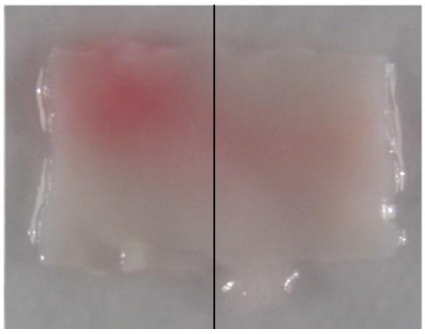

(28)

Figure 4.7.27. Preprocessed OCT image of vascular tissue with atherosclerotic plaque from a 4 month old WHHLML rabbit at 120th B-scan. Figure 4.7.28. Photographic image of vascular tissue with atherosclerotic from a 4 month old WHHLML rabbit.

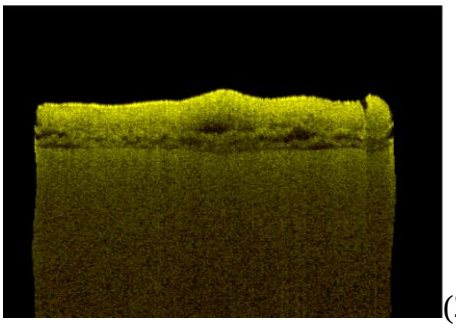

(29)

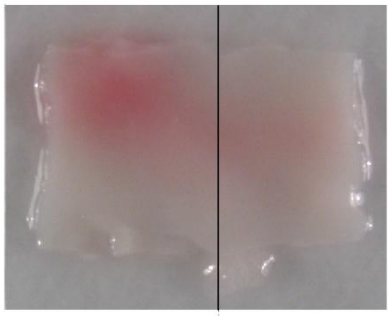

(30)

Figure 4.7.29. Preprocessed OCT image of vascular tissue with atherosclerotic plaque from a 4 month old WHHLML rabbit at 130th B-scan. Figure 4.7.30. Photographic image of vascular tissue with atherosclerotic from a 4 month old WHHLML rabbit.

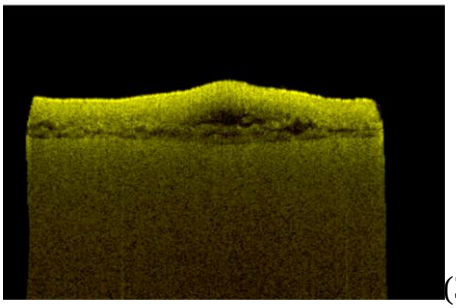

(31)

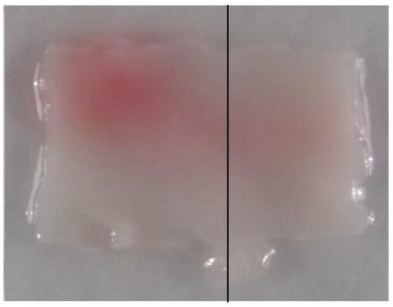

(32)

Figure 4.7.31. Preprocessed OCT image of vascular tissue with atherosclerotic plaque from a 4 month old WHHLML rabbit at 140th B-scan. Figure 4.7.32. Photographic image of vascular tissue with atherosclerotic from a 4 month old WHHLML rabbit.

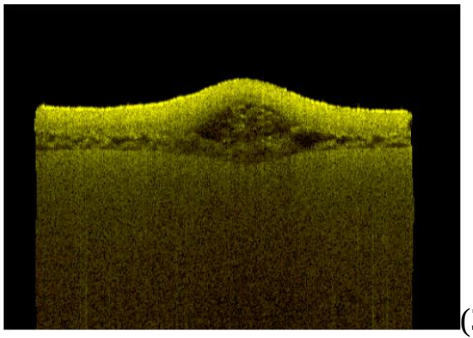

(33)

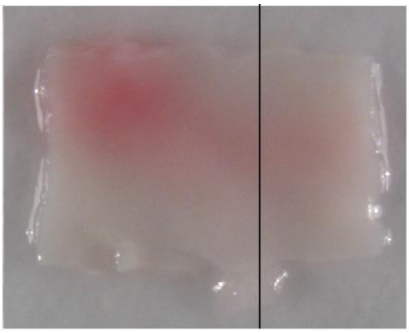

(34)

Figure 4.7.33. Preprocessed OCT image of vascular tissue with atherosclerotic plaque from a 4 month old WHHLML rabbit at 150th B-scan. Figure 4.7.34. Photographic image of vascular tissue with atherosclerotic from a 4 month old WHHLML rabbit.

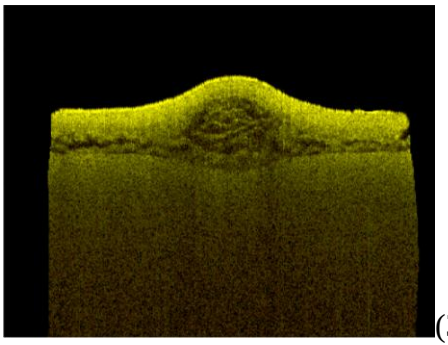

(35)

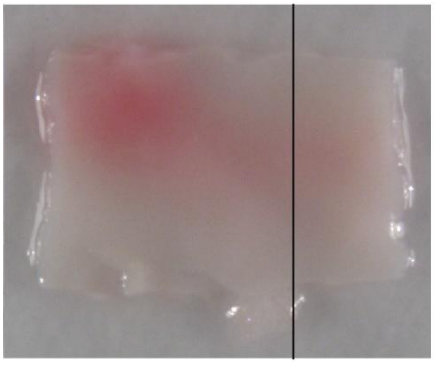

(36)

Figure 4.7.35. Preprocessed OCT image of vascular tissue with atherosclerotic plaque from a 4 month old WHHLML rabbit at 160th B-scan. Figure 4.7.36. Photographic image of vascular tissue with atherosclerotic from a 4 month old WHHLML rabbit.

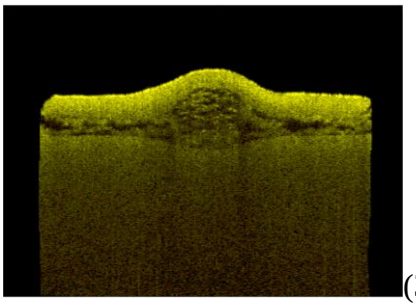
(37)

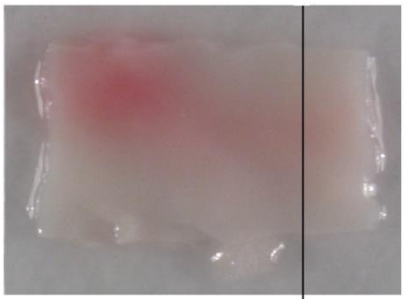
(38)

Figure 4.7.37. Preprocessed OCT image of vascular tissue with atherosclerotic plaque from a 4 month old WHHLML rabbit at 170th B-scan. Figure 4.7.38. Photographic image of vascular tissue with atherosclerotic from a 4 month old WHHLML rabbit.

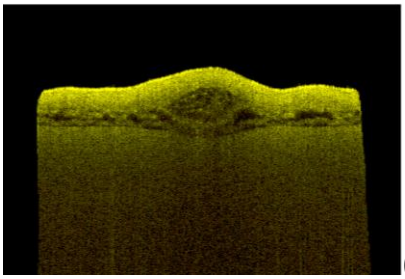
(39)

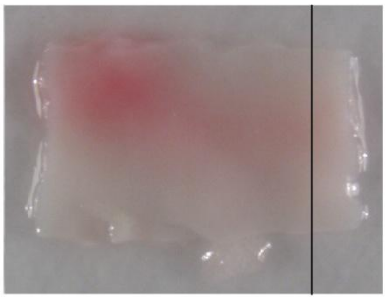
(40)

Figure 4.7.39. Preprocessed OCT image of vascular tissue with atherosclerotic plaque from a 4 month old WHHLML rabbit at 180th B-scan. Figure 4.7.40. Photographic image of vascular tissue with atherosclerotic from a 4 month old WHHLML rabbit.

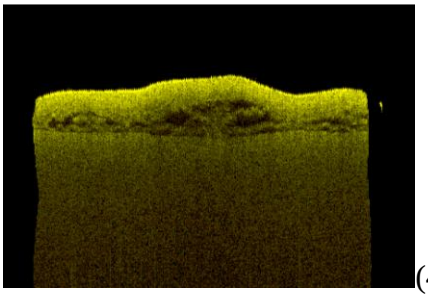
(41)

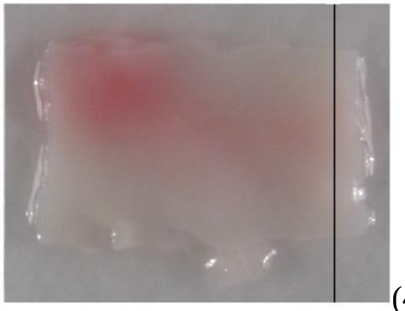
(42)

Figure 4.7.41. Preprocessed OCT image of vascular tissue with atherosclerotic plaque from a 4 month old WHHLML rabbit at 190th B-scan. Figure 4.7.42. Photographic image of vascular tissue with atherosclerotic from a 4 month old WHHLML rabbit.

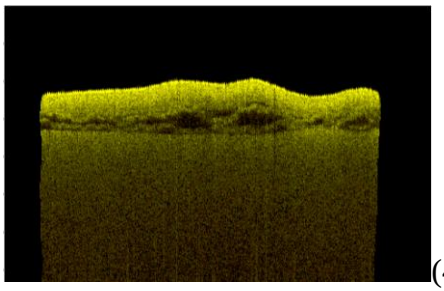
(43)

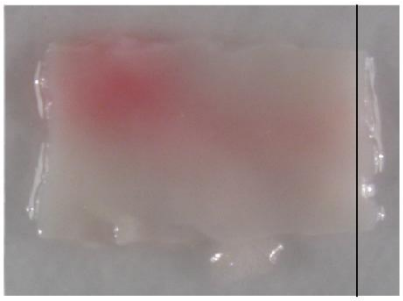
(44)

Figure 4.7.43. Preprocessed OCT image of vascular tissue with atherosclerotic plaque from a 4 month old WHHLML rabbit at 200th B-scan. Figure 4.7.44. Photographic image of vascular tissue with atherosclerotic from a 4 month old WHHLML rabbit.

Testing Images of class A (14 Images)

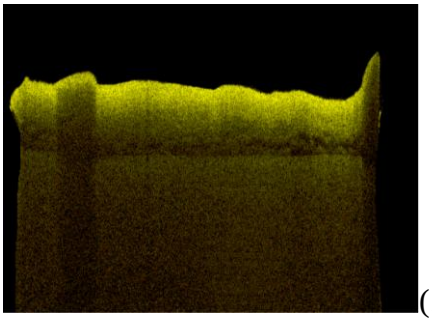
(1)

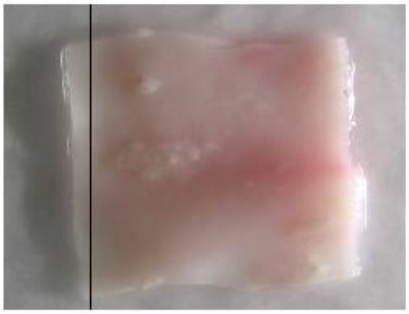
(2)

Figure 4.8.1. Preprocessed OCT image of vascular tissue with atherosclerotic plaque from a 4 month old WHHLML rabbit at 60th B-scan. Figure 4.8.2. Photographic image of vascular tissue with atherosclerotic from a 4 month old WHHLML rabbit.

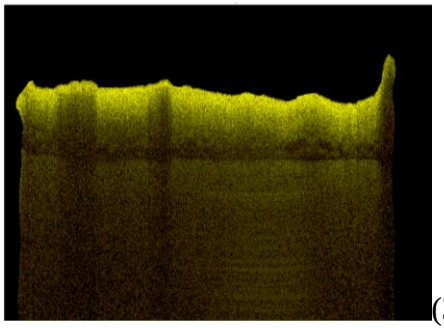

(3)

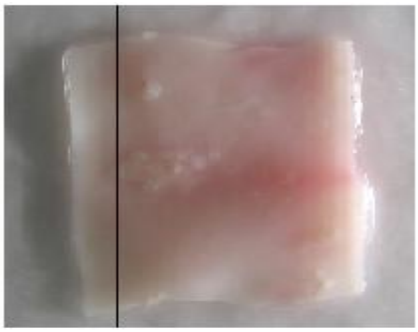

(4)

Figure 4.8.3. Preprocessed OCT image of vascular tissue with atherosclerotic plaque from a 4 month old WHHLML rabbit at 70th B-scan. Figure 4.8.4. Photographic image of vascular tissue with atherosclerotic from a 4 month old WHHLML rabbit.

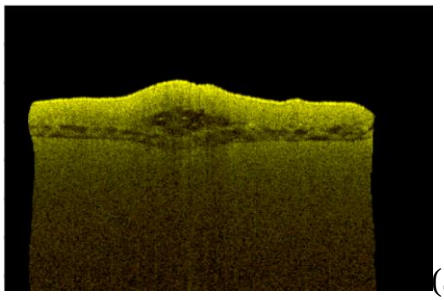

(5)

(6)

Figure 4.8.5. Preprocessed OCT image of vascular tissue with atherosclerotic plaque from a 4 month old WHHLML rabbit at 80th B-scan. Figure 4.8.6. Photographic image of vascular tissue with atherosclerotic from a 4 month old WHHLML rabbit.

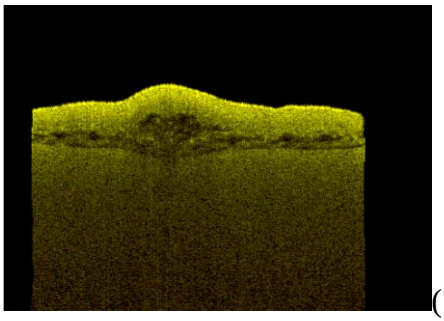

(7)

(8)

Figure 4.8.7. Preprocessed OCT image of vascular tissue with atherosclerotic plaque from a 4 month old WHHLML rabbit at 90th B-scan. Figure 4.8.8. Photographic image of vascular tissue with atherosclerotic from a 4 month old WHHLML rabbit.

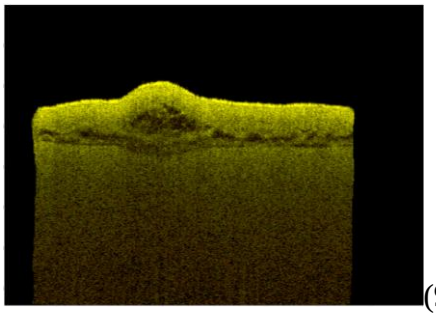

(9)

(10)

Figure 4.8.9. Preprocessed OCT image of vascular tissue with atherosclerotic plaque from a 4 month old WHHLML rabbit at 100th B-scan. Figure 4.8.10. Photographic image of vascular tissue with atherosclerotic from a 4 month old WHHLML rabbit.

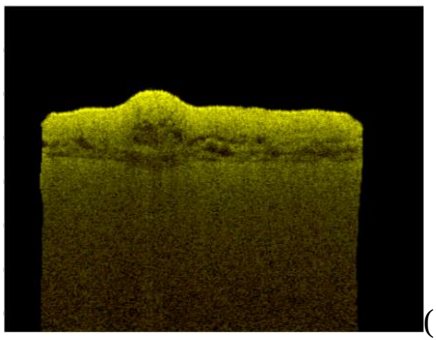

(11)

(12)

Figure 4.8.11. Preprocessed OCT image of vascular tissue with atherosclerotic plaque from a 4 month old WHHLML rabbit at 110th B-scan. Figure 4.8.12. Photographic image of vascular tissue with atherosclerotic from a 4 month old WHHLML rabbit.

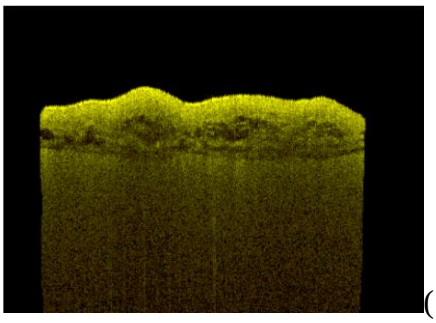

(13)

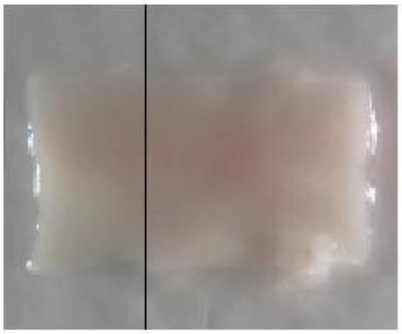

(14)

Figure 4.8.13. Preprocessed OCT image of vascular tissue with atherosclerotic plaque from a 4 month old WHHLML rabbit at 120th B-scan. Figure 4.8.14. Photographic image of vascular tissue with atherosclerotic from a 4 month old WHHLML rabbit.

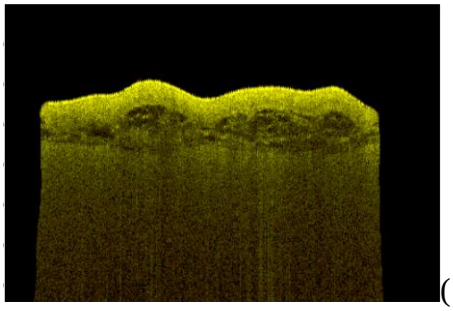
(15)

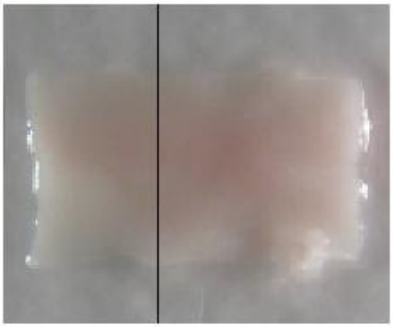
(16)

Figure 4.8.15. Preprocessed OCT image of vascular tissue with atherosclerotic plaque from a 4 month old WHHLML rabbit at 130th B-scan. Figure 4.8.16. Photographic image of vascular tissue with atherosclerotic from a 4 month old WHHLML rabbit.

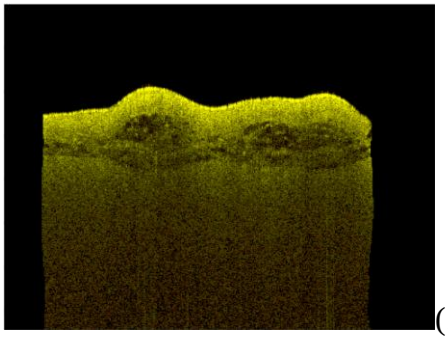
(17)


(18)

Figure 4.8.17. Preprocessed OCT image of vascular tissue with atherosclerotic plaque from a 4 month old WHHLML rabbit at 140th B-scan. Figure 4.8.18. Photographic image of vascular tissue with atherosclerotic from a 4 month old WHHLML rabbit.

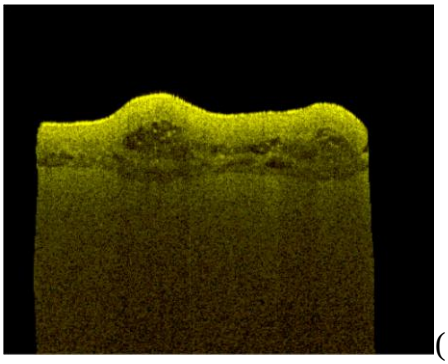

(19)

(20)

Figure 4.8.19. Preprocessed OCT image of vascular tissue with atherosclerotic plaque from a 4 month old WHHLML rabbit at 150th B-scan. Figure 4.8.20. Photographic image of vascular tissue with atherosclerotic from a 4 month old WHHLML rabbit.

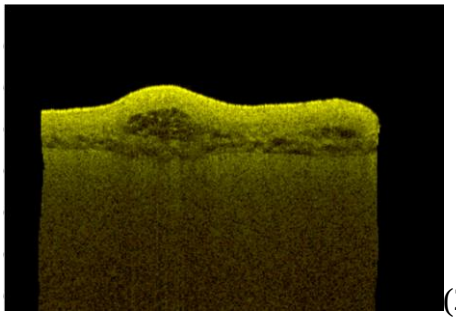

(21)

(22)

Figure 4.8.21. Preprocessed OCT image of vascular tissue with atherosclerotic plaque from a 4 month old WHHLML rabbit at 160th B-scan. Figure 4.8.22. Photographic image of vascular tissue with atherosclerotic from a 4 month old WHHLML rabbit.

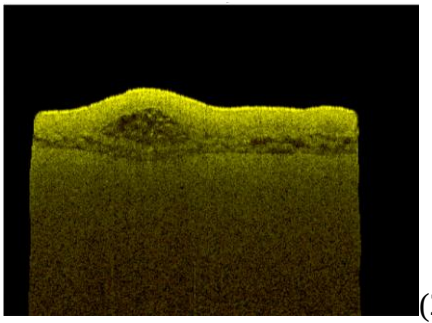

(23)

(24)

Figure 4.8.23. Preprocessed OCT image of vascular tissue with atherosclerotic plaque from a 4 month old WHHLML rabbit at 170th B-scan. Figure 4.8.24. Photographic image of vascular tissue with atherosclerotic from a 4 month old WHHLML rabbit.

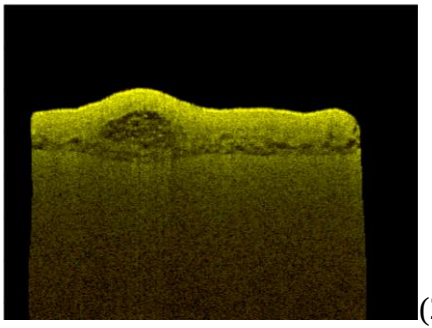

(25)

(26)

Figure 4.8.25. Preprocessed OCT image of vascular tissue with atherosclerotic plaque from a 4 month old WHHLML rabbit at 180th B-scan. Figure 4.8.26. Photographic image of vascular tissue with atherosclerotic from a 4 month old WHHLML rabbit.

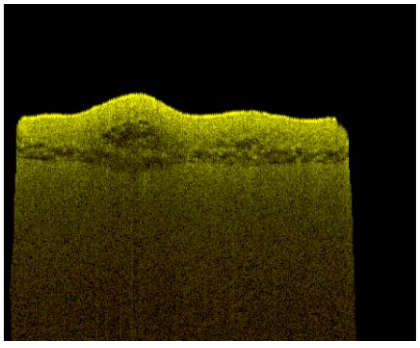

(27)

(28)

Figure 4.8.27. Preprocessed OCT image of vascular tissue with atherosclerotic plaque from a 4 month old WHHLML rabbit at 190th B-scan. Figure 4.8.28. Photographic image of vascular tissue with atherosclerotic from a 4 month old WHHLML rabbit.

CHAPTER 5: DETECTION OF ATHEROSCLEROTIC PLAQUE USING UNSUPERVISED ALGORITHM

5.1 Introduction

In the previous chapter, we described classification of atherosclerosis using supervised classification. In this chapter, we turn to unsupervised case, where the class labels of the dataset are unknown. Thus the concern now is to organize the dataset into sensible clusters or groups, which will help in finding the similarities or difference in the dataset. Unsupervised classification is also known as clustering analysis. The illustration of supervised and unsupervised classification is given below, Figure 5.1.a describes the supervised classification of training set {(x1, y1) (x2,y2) }, where x1,x2 are data points and y1,y2 are class labels and figure 5.1.b describes the unsupervised case where the x1, x2 are the data points but the class labels are unknown.

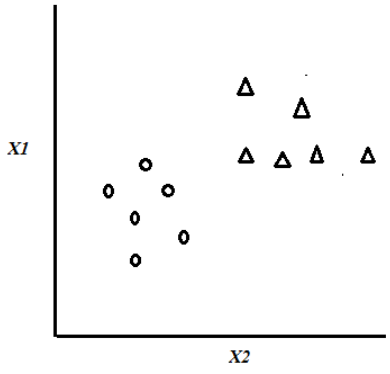

Figure 5.1.a Example of supervised case

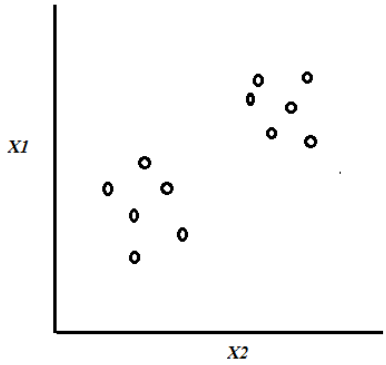

Figure 5.1.b Example of unsupervised case

In this chapter we described the preliminary study using SGLDM method along with clustering algorithm to detect the atherosclerotic plaque region from normal tissue on OCT images. In spite of high resolution of OCT images, visual classification of vascular tissue and plaque regions is not easy. However examination of such OCT images reveals that they frequently display a characteristics texture due to speckle [14]. In this chapter, we show that the detection of atherosclerotic plaque on OCT vascular images based on the texture segmentation using clustering algorithm can be carried out successfully without reliance on visible structures.

To the author's knowledge, detection of atherosclerotic plaque on OCT image based on texture segmentation has not been performed previously. However literature exists on atherosclerotic plaque segmentation using Intravascular Ultrasound (IVUS) [98], computed tomography (CT) [99] and Magnetic resonance Imaging (MRI) [100]. OCT offers a combination of micron-scale morphological imaging with penetration depths of 1~3 mms which makes it unique among other imaging modalities.

Texture segmentation is the process of identifying different regions based on their texture. The statistical properties of the texture can be measured by the region histograms and their moments. There are different methods to extract texture features using statistical technologies. There exist a large body of literature for texture feature extraction using the gray level difference method (GLDM), the gray level run length method (GLRLM), and the power spectral method (PSM) [101-103]. However studies have shown that the Spatial Gray level dependent matrix (SGLDM) method is the most powerful texture feature extraction method [104].

Our unsupervised method is divided into following five sections,

1. Preprocessing of our raw OCT vascular images.

2. Extraction of statistical texture features.

3. Feature normalization and mapping the extracted features back to original image.

4. Classification using supervised learning algorithm (*Knn*).

5. Validation using actual photographic images.

5.2 Preprocessing of our raw OCT vascular images

Our raw OCT vascular images contained floating point numbers, so we performed segmentation using image normalization on each image file to achieve a uniform distribution of intensities on a standardized intensity range and to improve contrast. After image normalization, each pixel has a brightness value ranging from 0 to 255. This was performed by Min-Max normalization operation. It preserves all relationships of the data values exactly. It would compress the normal range if extreme values or outliers exist. Min-Max normalization is carried using the following formula:

$$\text{Image} = \frac{\min(\text{Image})}{\max(\text{Image})\text{-}\min(\text{Image})} \times 255 \tag{5.1}$$

After normalizing our image file, we performed automatic image segmentation using a threshold to improve the image quality.

5. 3 Extraction of statistical texture feature

We extracted texture features on our processed OCT vascular images using SGLDM method, which is a known method for extracting second order statistical texture features. Features derived from the SGLDM method have been widely used for classification of tissue images [83-87]. Rosenfeld and Troy [88] and Haralick et al. [89] first proposed SGLDM matrices for arbitrary spatial distances and angular directions. The two parameters used to construct SGLDM matrices are 1. Relative distance among image pixels, d and 2. Relative orientation among pixels, $\boldsymbol{\theta}$.

The SGLDM method determines the probability of occurrence of grey levels with respect to relative spatial pixel positions in an image. The SGLDM matrices are based on an estimate of second-order joint conditional probability density functions p (i, j: d, θ) [90-93]. These probability density functions, p (i, j: d, θ), measure the probability that two pixels, which are located with an inter sample distance, d and direction, θ, have gray levels i and j. To detect the atherosclerotic plaque using these SGLDMs, we extracted 11 texture features in two directions

We calculated the features from SGLDM matrices as shown table 4.1

5.4 Feature normalization

The scale of the features lied within a different dynamic range. We normalized the entire 22 feature vector. Feature normalization ensures that all the features have same influence on performance of the classifier. Each feature vector of an image is normalized as follows:

$$\hat{x} = \frac{x - \bar{x}}{\sigma} \tag{5.2}$$

Where, $\hat{x}$ is the normalized value, x is the raw feature vector, $\bar{x}$ is the sample mean and σ is the standard deviation.

5.5 Unsupervised clustering algorithm

After feature normalization, we carried out atherosclerotic plaque detection on OCT images using K-means clustering algorithm [105], which is considered as a popular clustering techniques due to its simplicity and fast convergence. We applied K-means clustering algorithm on the feature space to segment the air, plaque and healthy vascular tissue regions and mapped the segmented features back to original image.

The K-means algorithm generally requires four parameters: (1) number of clusters; (2) a distance metric; (3) Initialization of cluster centroids and (4) a convergence criterion. Figure 5.1 shows an illustration of k -means clustering .

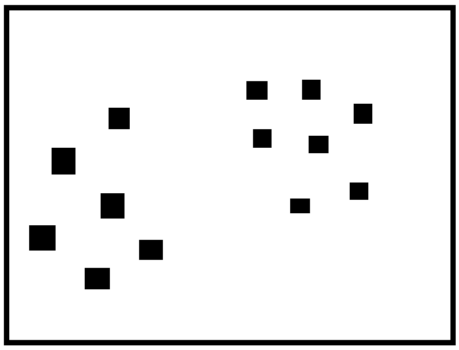

Figure 5.2.a Original dataset

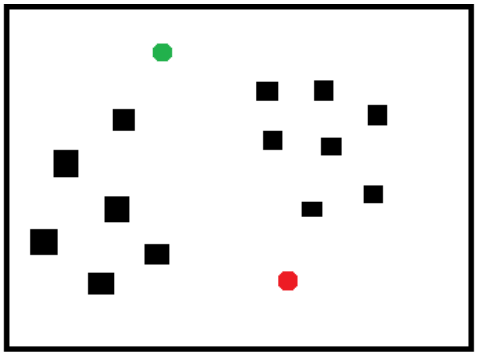

Figure 5.2.b Random Initialization of cluster centroids

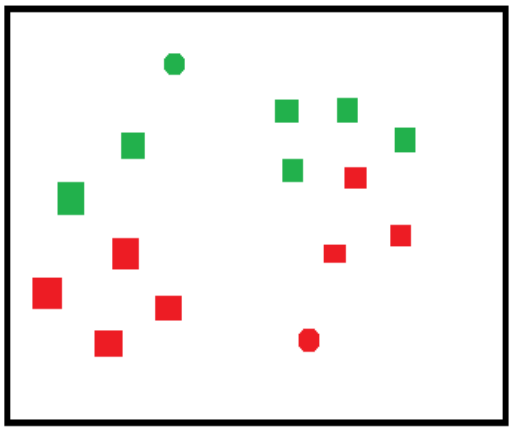

Figure 5.2.c Assigning data points to the to the closest cluster centroid

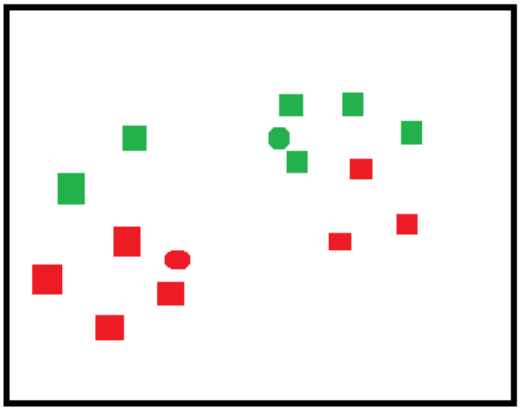

Figure 5.2.d Moving each cluster centroid to the mean of the points assigned to it.

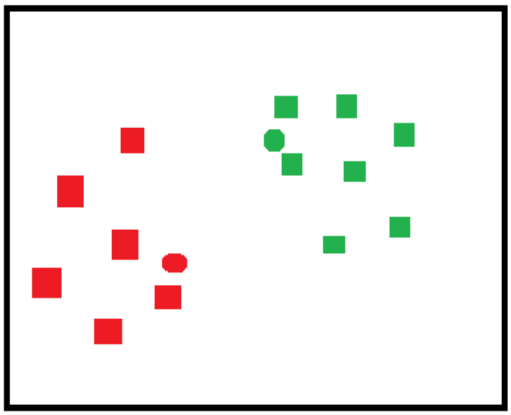

Figure.5.2.d Again assigning data points to the to the closest cluster centroid

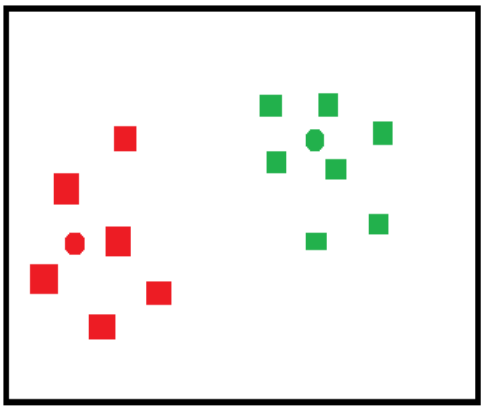

Figure.5.2.e Moving each cluster centroid to the mean of the points assigned to it.

K means algorithm works in two steps:

Inputs to K means classifier are

1. Training data set = { $x_1, x_2, \ldots\ldots x_k$}
2. Number of cluster (*K*)

Step 1 : Initialization of cluster centroids m_1, m_2, m_3.. m_n randomly.

Step 2: Repeat step 2 until convergence

{

find the distance between every data point and the cluster centroid, and then assign the data points x_i to the closet cluster centroid m_j.

For every i,

$$\mu_i \equiv \arg\min_j \left\| x_i - m_j \right\| \qquad 5.3$$

Moving each cluster centroid m_j to the mean of the data points assigned to it

For every j

$$m_j \equiv \frac{\sum_{i=1}^{k} 1\{\mu_i = j\} x_i}{\sum_{i=1}^{m} 1\{\mu_i = j\}} \qquad 5.4$$

1 denotes the indicator function.

As our OCT images consisted of regions representing air, plaque, and healthy vascular tissue and air, we selected the number of clusters, K=3. We defined distance between each cluster by a Euclidean distance metric and initialized cluster centroid randomly. The dataset in feature space was initially partitioned into 3 clusters and the data points were randomly assigned to the cluster centroid. For each data point, we calculated the city block distance from the data point to cluster centroid. If the data point was not closest to its own cluster, it was to be shifted into the closest cluster. Otherwise, the data point was not shifted. The process continued until convergence was achieved.

5.6 Validation

The results of segmentation show that the plaque region on OCT images could be detected correctly. For validation, we compared our resulting segmented OCT images with different locations on photographic images of vascular tissue with atherosclerotic plaque. As shown in Fig. 5.3, Fig. 5.4, Fig. 5.5, Fig. 5.6, Fig. 5.7, Fig. 5.8, Fig. 5.9 and Fig. 5.10 (with window sizes of 32×32) both plaque and healthy tissue regions were correctly segmented. The highlighted area on all the OCT images is the detected atherosclerotic plaque regions.

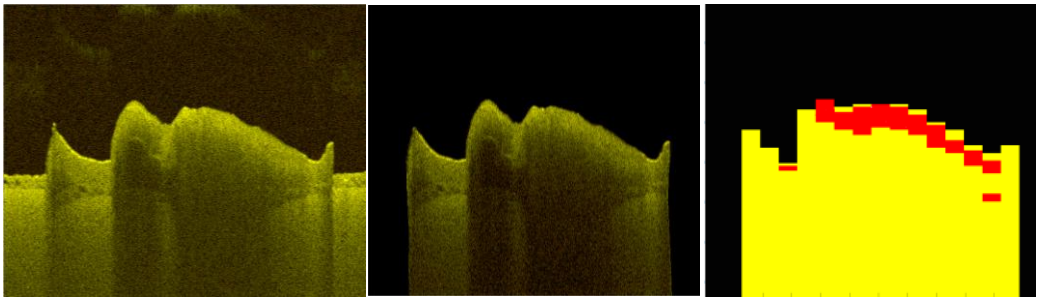

(a) (b) (c)

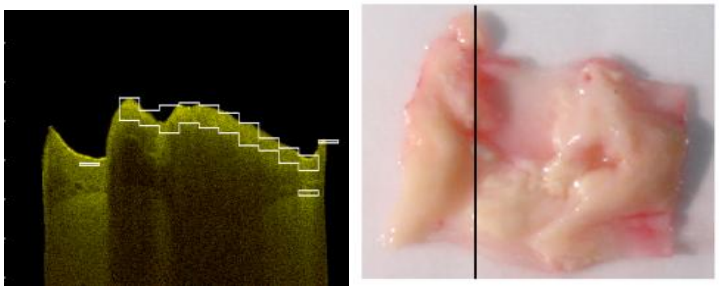

(d) (e)

Figure 5.3.(a) Raw OCT image of vascular tissue with atherosclerotic plaque from a 10 month old WHHLML rabbit at 100th B-scan (b) Preprocessed OCT image of vascular tissue with atherosclerotic plaque from a 10 month old WHHLML rabbit at 100th B-scan(c) Results of our unsupervised clustering showing three different classes (d) Plaque detection result OCT image of vascular tissue with atherosclerotic plaque from a 10 month old WHHLML rabbit at 100th B-scan(e) Photographic image of vascular tissue with atherosclerotic from a 10 month old WHHLML rabbit.

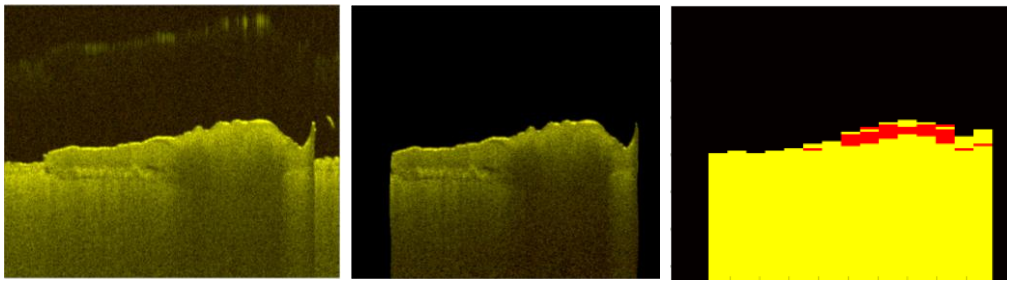

(a) (b) (c)

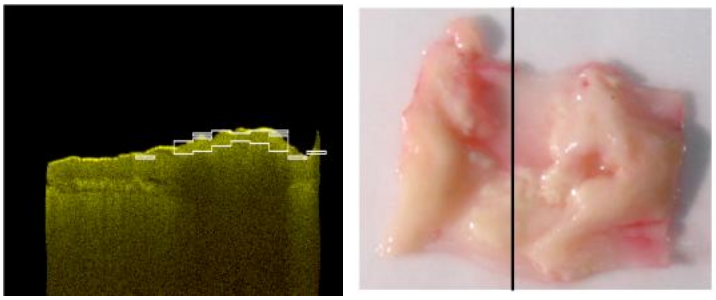

(d) (e)

Figure 5.4 (a) Raw OCT image of vascular tissue with atherosclerotic plaque from a 10 month old WHHLML rabbit at 150th B-scan (b) Preprocessed OCT image of vascular tissue with atherosclerotic plaque from a 10 month old WHHLML rabbit at 150th B-scan(c) Results of our unsupervised clustering showing three different classes (d) Plaque detection result OCT image of vascular tissue with atherosclerotic plaque from a 10 month old WHHLML rabbit at 150th B-scan(e) Photographic image of vascular tissue with atherosclerotic from a 10 month old WHHLML rabbit.

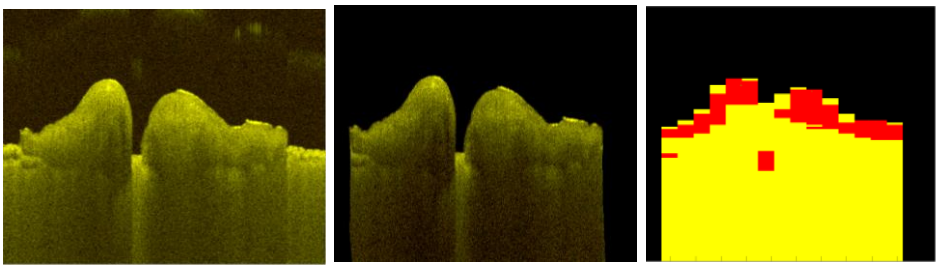

(a) (b) (c)

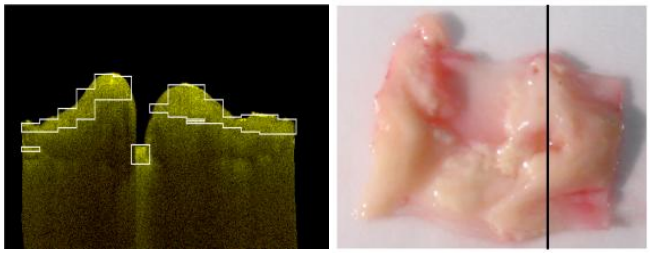

(d) (e)

Figure 5.5 (a) Raw OCT image of vascular tissue with atherosclerotic plaque from a 10 month old WHHLML rabbit at 250th B-scan (b) Preprocessed OCT image of vascular tissue with atherosclerotic plaque from a 10 month old WHHLML rabbit at 250th B-scan(c) Results of our unsupervised clustering showing three different classes (d) Plaque detection result OCT image of vascular tissue with atherosclerotic plaque from a 10 month old WHHLML rabbit at 250th B-scan(e) Photographic image of vascular tissue with atherosclerotic from a 10 month old WHHLML rabbit.

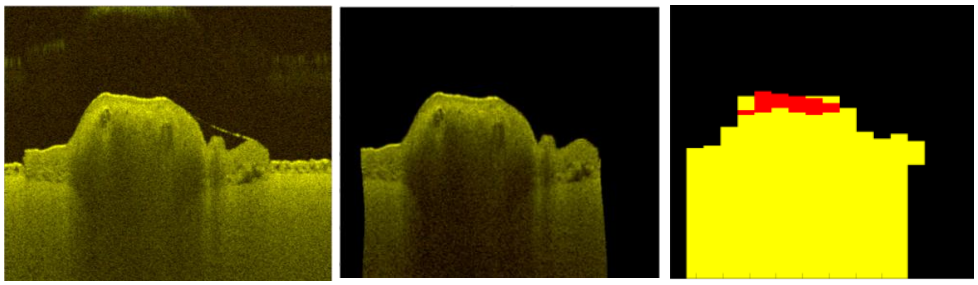

(a) (b) (c)

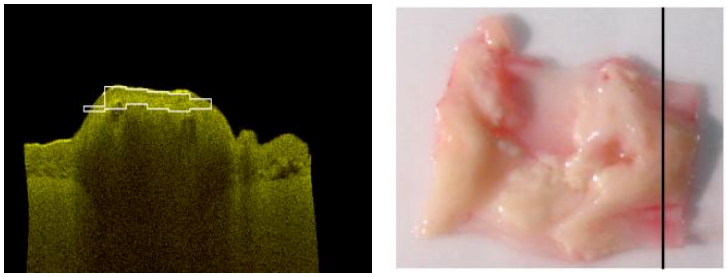

(d) (e)

Figure 5.6 (a) Raw OCT image of vascular tissue with atherosclerotic plaque from a 10 month old WHHLML rabbit at 300th B-scan (b) Preprocessed OCT image of vascular tissue with atherosclerotic plaque from a 10 month old WHHLML rabbit at 300th B-scan(c) Results of our unsupervised clustering showing three different classes (d) Plaque detection result OCT image of vascular tissue with atherosclerotic plaque from a 10 month old WHHLML rabbit at 300th B-scan(e) Photographic image of vascular tissue with atherosclerotic from a 10 month old WHHLML rabbit.

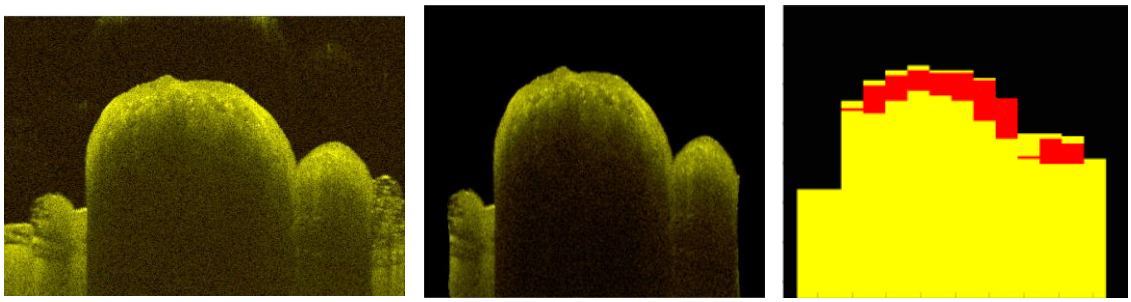

(a) (b) (c)

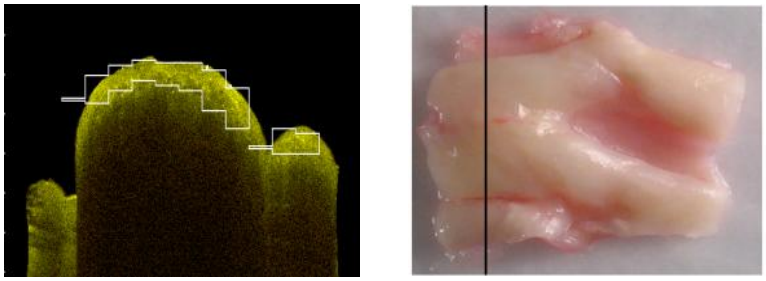

(d) (e)

Figure 5.7 (a) Raw OCT image of vascular tissue with atherosclerotic plaque from a 19 month old WHHLML rabbit at 60th B-scan (b) Preprocessed OCT image of vascular tissue with atherosclerotic plaque from a 10 month old WHHLML rabbit at 60th B-scan(c) Results of our unsupervised clustering showing three different classes (d) Plaque detection result OCT image of vascular tissue with atherosclerotic plaque from a 10 month old WHHLML rabbit at 60th B-scan(e) Photographic image of vascular tissue with atherosclerotic from a 10 month old WHHLML rabbit.

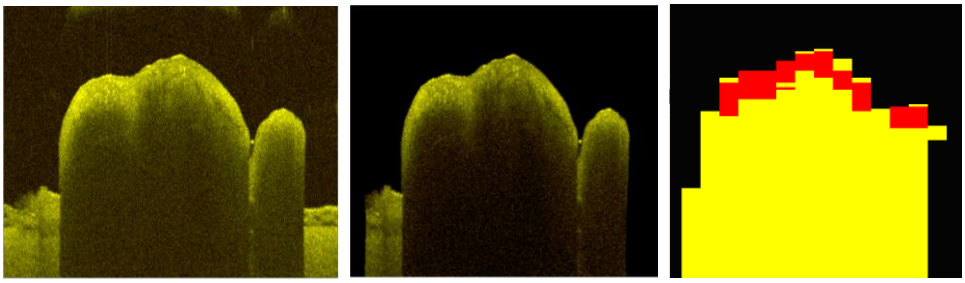

(a) (b) (c)

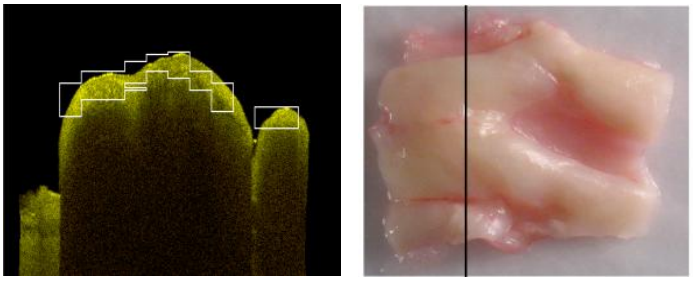

(d) (e)

Figure 5.8 (a) Raw OCT image of vascular tissue with atherosclerotic plaque from a 19 month old WHHLML rabbit at 100th B-scan (b) Preprocessed OCT image of vascular tissue with atherosclerotic plaque from a 10 month old WHHLML rabbit at 100th B-scan(c) Results of our unsupervised clustering showing three different classes (d) Plaque detection result OCT image of vascular tissue with atherosclerotic plaque from a 10 month old WHHLML rabbit at 100th B-scan(e) Photographic image of vascular tissue with atherosclerotic from a 10 month old WHHLML rabbi

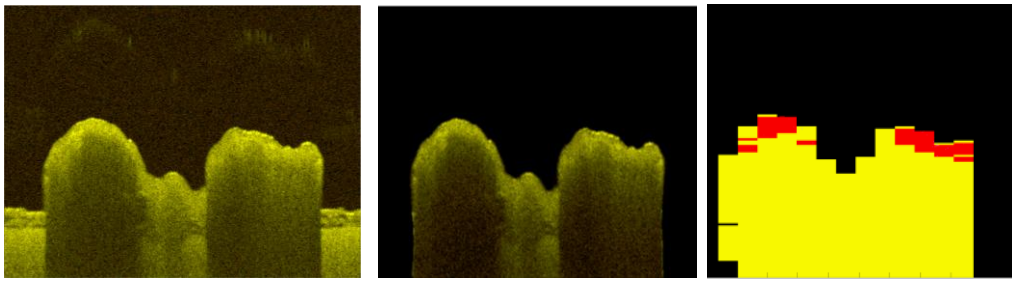

(a) (b) (c)

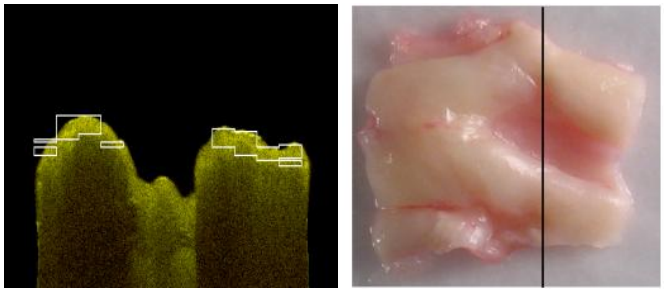

(d) (e)

Figure 5.9 (a) Raw OCT image of vascular tissue with atherosclerotic plaque from a 19 month old WHHLML rabbit at 180th B-scan (b) Preprocessed OCT image of vascular tissue with atherosclerotic plaque from a 10 month old WHHLML rabbit at 180th B-scan(c) Results of our unsupervised clustering showing three different classes (d) Plaque detection result OCT image of vascular tissue with atherosclerotic plaque from a 10 month old WHHLML rabbit at 180th B-scan(e) Photographic image of vascular tissue with atherosclerotic from a 10 month old WHHLML rabbit

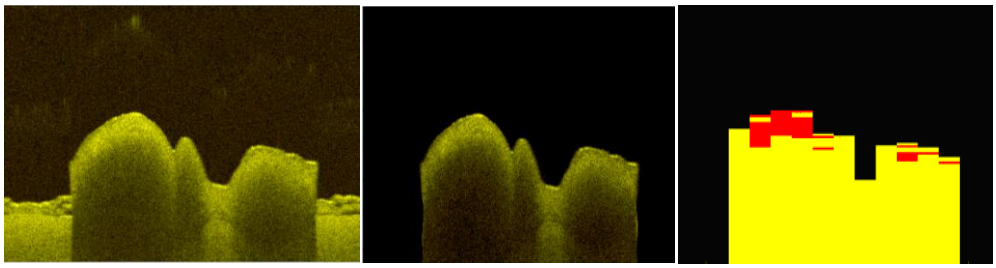

(a) (b) (c)

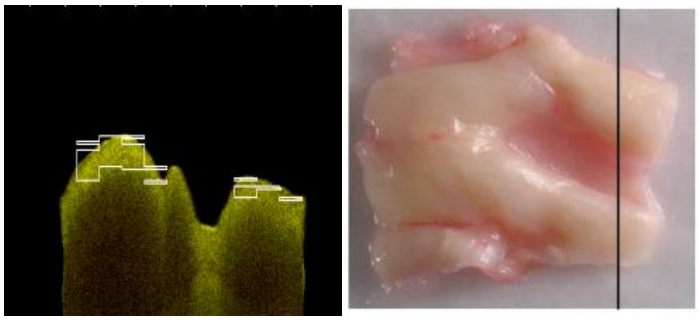

(d) (e)

Figure 5.10 (a) Raw OCT image of vascular tissue with atherosclerotic plaque from a 19 month old WHHLML rabbit at 230th B-scan (b) Preprocessed OCT image of vascular tissue with atherosclerotic plaque from a 10 month old WHHLML rabbit at 230th B-scan(c) Results of our unsupervised clustering showing three different classes (d) Plaque detection result OCT image of vascular tissue with atherosclerotic plaque from a 10 month old WHHLML rabbit at 230th B-scan(e) Photographic image of vascular tissue with atherosclerotic from a 10 month old WHHLML rabbit

In following section we demonstrated plaque detection with different window sizes.

Figure 5.11 shows the demonstration with window size of 16×16

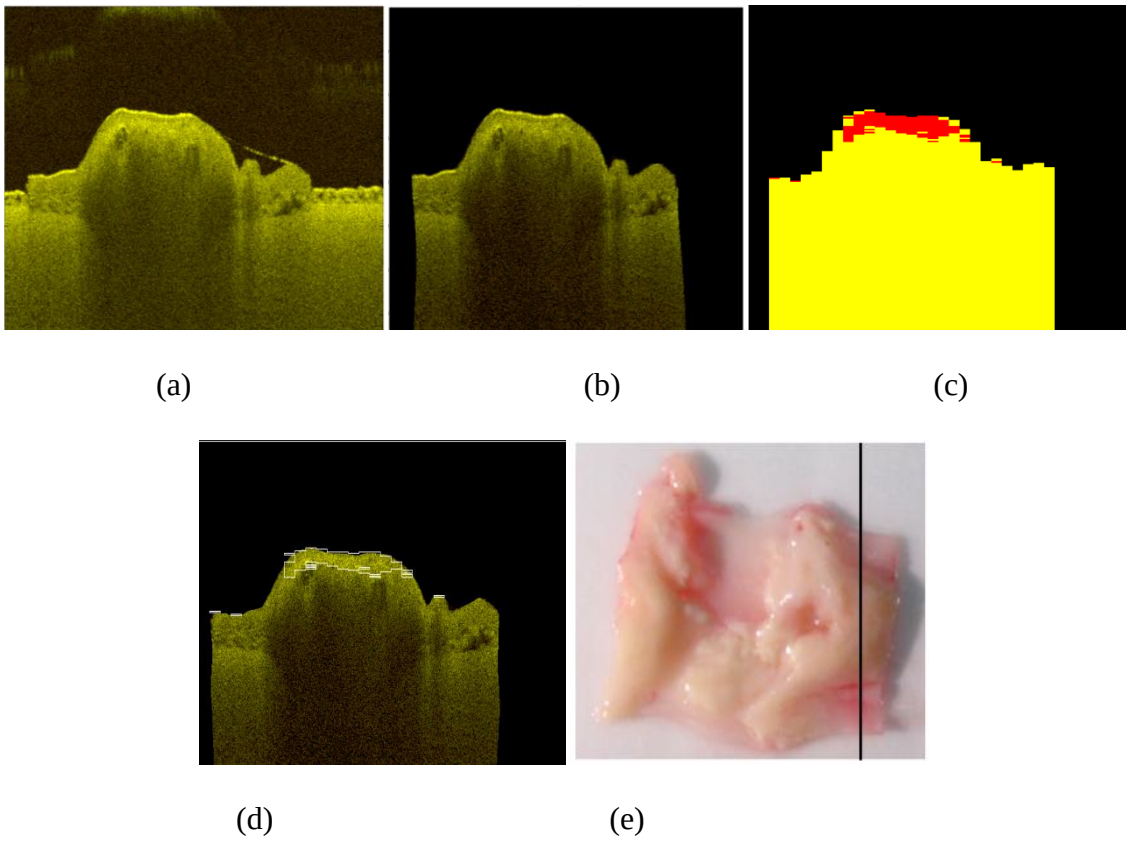

(a) (b) (c)

(d) (e)

Figure 5.11 (a) Raw OCT image of vascular tissue with atherosclerotic plaque from a 10 month old WHHLML rabbit at 300th B-scan (b) Preprocessed OCT image of vascular tissue with atherosclerotic plaque from a 10 month old WHHLML rabbit at 300th B-scan(c) Results of our unsupervised clustering showing three different classes (d) Plaque detection result OCT image of vascular tissue with atherosclerotic plaque from a 10 month old WHHLML rabbit at 300th B-scan(e) Photographic image of vascular tissue with atherosclerotic from a 10 month old WHHLML rabbit.

Figure 5.12 shows the demonstration with window size of 8×8

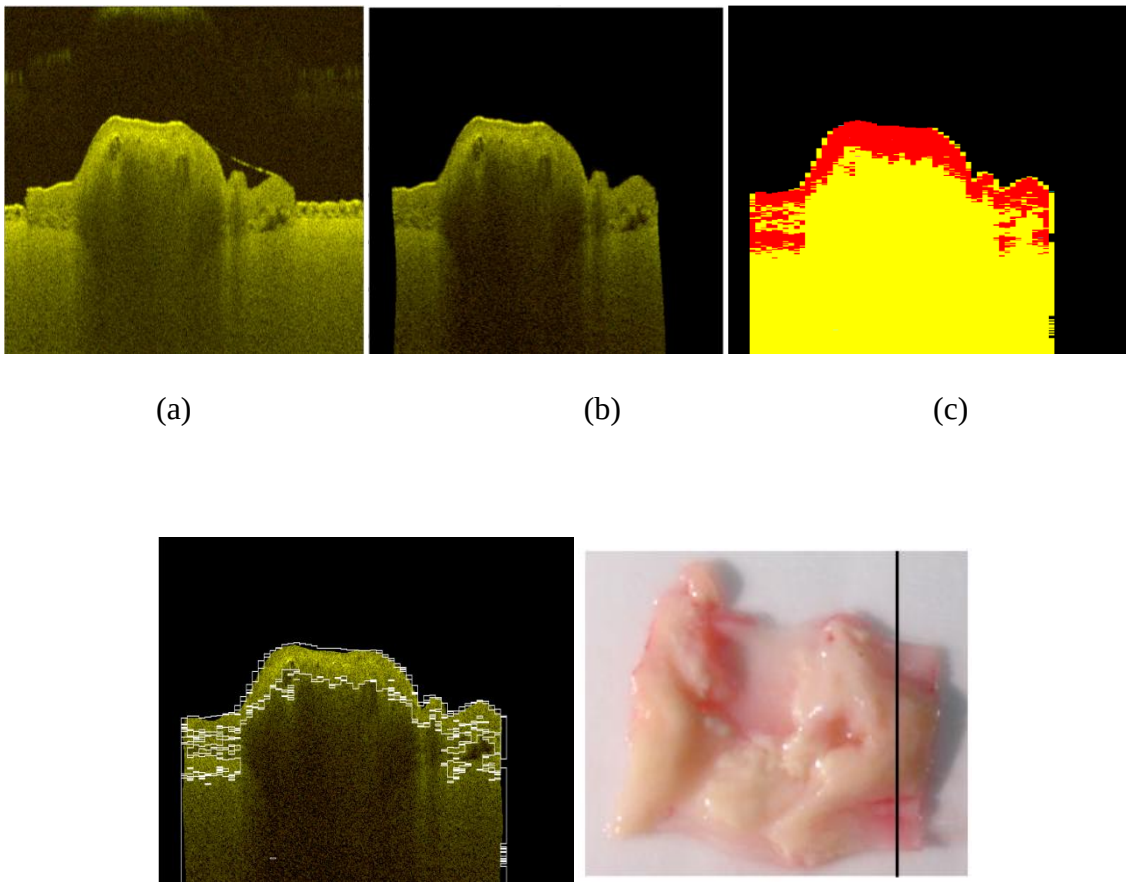

(a) (b) (c)

(d) (e)

Figure 5.12 (a) Raw OCT image of vascular tissue with atherosclerotic plaque from a 10 month old WHHLML rabbit at 300th B-scan (b) Preprocessed OCT image of vascular tissue with atherosclerotic plaque from a 10 month old WHHLML rabbit at 300th B-scan(c) Results of our unsupervised clustering showing three different classes (d) Plaque detection result OCT image of vascular tissue with atherosclerotic plaque from a 10 month old WHHLML rabbit at 300th B-scan(e) Photographic image of vascular tissue with atherosclerotic from a 10 month old WHHLML rabbit.

Figure 5.13 shows the demonstration with window size of 64×64

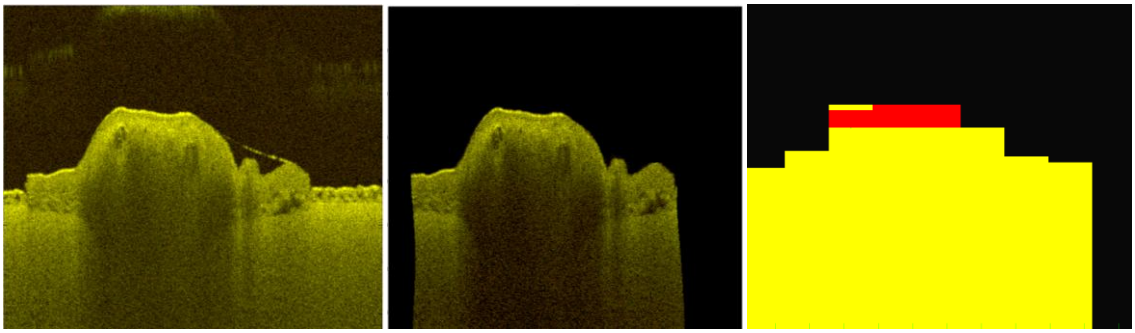

(a) (b) (c)

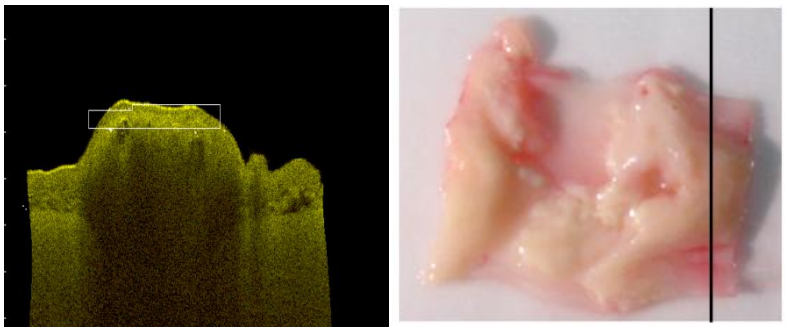

(d) (e)

Figure 5.13 (a) Raw OCT image of vascular tissue with atherosclerotic plaque from a 10 month old WHHLML rabbit at 300th B-scan (b) Preprocessed OCT image of vascular tissue with atherosclerotic plaque from a 10 month old WHHLML rabbit at 300th B-scan(c) Results of our unsupervised clustering showing three different classes (d) Plaque detection result OCT image of vascular tissue with atherosclerotic plaque from a 10 month old WHHLML rabbit at 300th B-scan(e) Photographic image of vascular tissue with atherosclerotic from a 10 month old WHHLML rabbit.

In this chapter we implemented an automated unsupervised learning algorithm which incorporates an unsupervised learning using K-means clustering, to detect the plaque region from OCT vascular images of tissue. Our method extracted the texture features of the OCT vascular images based on their statistics rather than the visible structure. Our results show excellent matching with actual photographs of vascular tissue with atherosclerotic plaque. To the best of our knowledge, this is the first automated method to detect atherosclerotic plaque from OCT images of vascular tissue. Our plaque detection approach is an important prerequisite to assess plaque vulnerability clinically. The ability of our method to detect invisible change in tissue structure could have significant impact to help diagnosis of atherosclerosis disease.

CHAPTER 6: CONCLUSION AND FUTURE WORK

In this thesis, we presented two different methods to classify atherosclerotic plaque on OCT vascular images without reliance on visible structures.

We performed classification of atherosclerosis using automatic supervised classification technique and detection of atherosclerosis using unsupervised learning algorithm based on texture analysis. We achieved excellent classification and segmentation result in both supervised and unsupervised methods. Therefore our proposed plaque detection technique could be potentially used in clinical cardiovascular OCT imaging.

We performed supervised classification of atherosclerotic plaque by employing a non parametric classifier (*Knn* classifier). This method consists of feature extraction process, feature normalization, feature selection process and finally the design of the classifier. The feature extraction process was carried using SGLDM method, which is known to the best method to extract texture features [14]. Since the scale of all the features varied dynamically, we normalized them using a min-min normalization operation. To reduce the dimension of feature space and to ensure good generalization of our classifier, we employed feature selection process. Our feature selection process is further divided into three methods, 1. Scalar feature selection, 2. Feature selection by using cross correlation measure, 3. Finding the group of final set of features.

In scalar feature selection process, we consider each feature independently. To carry out scalar feature selection, we used Fisher discriminant ratio as cost function. We ranked all the features in descending order using scalar feature selection based our already

defined cost function. We then calculated the cross correlation between the pairs of all the features and found the top 16 features out of 22 set of features. To further reduce the dimension of our feature space, we carried an exhaustive search method, to find the combination of 5 best features. Finally we fed our group of final 5 features to *k-nn* classifier. To validate our classification result employed a leave one out cross validation method. Our validation and classification error was only 4.54% and 10.4% respectively. The combination of OCT imaging modality and our proposed plaque detection technique can also be used as prerequisite to assess the plaque vulnerability clinically. Therefore our proposed method could be used to help clinicians in diagnosis of atherosclerosis disease. To the best of our knowledge, this is the first attempt to perform automated classification of atherosclerosis on OCT images without relying on its visible structural features. In future work, our supervised classifier can be extended to handle real time atherosclerosis detection application. It can also extend our classifier to differentiate different types of plaques associated with coronary arties disease and to quantify plaque burden.

We also developed an automatic unsupervised technique to detect atherosclerosis from OCT vascular images of tissues. Our method involves extraction of statistical textural features using the Spatial Gray Level Dependence Matrix (SGLDM) method, application of an unsupervised clustering algorithm (*K-means*) on the these features, and mapping of the segmented regions of features back to the actual image. We verified the validity of our results by visually comparing them to photographs of the vascular tissue with atherosclerotic plaque that we used to generate our OCT images.

The ability to detect atherosclerotic plaque from optical coherence tomography images by visual inspection is usually limited. It is further complicated by the high frame rates of modern intravascular OCT systems. The ability of our method to detect invisible change in tissue structure could have significant impact to help diagnosis of atherosclerosis disease using intravascular OCT imaging. Also, our proposed method can provide an important prerequisite to assess plaque burden clinically. To our knowledge, this is first automatic technique to detect atherosclerotic plaque based on unsupervised algorithm.

Future research may further help classify different types of plaque using OCT vascular images.

In this thesis we developed and implemented two techniques to classify atherosclerosis from OCT vascular images based on statistical texture features.

REFERENCES

[1] Statistics Canada. Morality, Summary List of Causes 2008. Released October 18, 2011

[2] S. Petersen, V. Peto, M. Rayner, J. Leal, R. Luengo-Fernandez, and A. Gray, "European cardiovascular disease statistics," *London: British Heart Foundation*, 2005.

[3] S. Allender, V. Peto, P. Scarborough, A. Kaur, and M. Rayner, *Coronary Heart Disease Statistics. London: British Heart Foundation; 2008*.

[4] Heart and Stroke Foundation report on Canadians health Ottawa, February 2011.

[5] R. Virmani, F. D. Kolodgie, A. P. Burke, A. Farb, and S. M. Schwartz, "Lessons from sudden coronary death a comprehensive morphological classification scheme for atherosclerotic lesions," *Arteriosclerosis, thrombosis, and vascular biology*, vol. 20, no. 5, pp. 1262–1275, 2000.

[6] Z. A. Fayad, V. Fuster, K. Nikolaou, and C. Becker, "Computed tomography and magnetic resonance imaging for noninvasive coronary angiography and plaque imaging," *Circulation*, vol. 106, no. 15, pp. 2026–2034, 2002.

[7] P. Felkel, R. Wegenkittl, and A. Kanitsar, "Vessel tracking in peripheral CTA datasets-an overview," in *Computer Graphics, Spring Conference on, 2001.*, 2001, pp. 232–239.

[8] I.-K. Jang, B. E. Bouma, D.-H. Kang, S.-J. Park, S.-W. Park, K.-B. Seung, K.-B. Choi, M. Shishkov, K. Schlendorf, and E. Pomerantsev, "Visualization of coronary atherosclerotic plaques in patients using optical coherence tomography: comparison with intravascular ultrasound," *Journal of the American College of Cardiology*, vol. 39, no. 4, pp. 604–609, 2002.

[9] A. Tanaka, T. Imanishi, H. Kitabata, T. Kubo, S. Takarada, H. Kataiwa, A. Kuroi, H. Tsujioka, T. Tanimoto, and N. Nakamura, "Distribution and frequency of thin-capped fibroatheromas and ruptured plaques in the entire culprit coronary artery in patients with acute coronary syndrome as determined by optical coherence tomography," *The American journal of cardiology*, vol. 102, no. 8, pp. 975–979, 2008.

[10] A. DE ROOS, L. J. KROFT, M. J. SCHALIJ, and J. H. REIBER, "Imaging of atherosclerosis: invasive and noninvasive techniques," *Hellenic J Cardiol*, vol. 50, pp. 245–263, 2009.

[11] E. Brunenberg, O. Pujol, B. ter Haar Romeny, and P. Radeva, "Automatic IVUS segmentation of atherosclerotic plaque with stop & go snake," *Medical Image Computing and Computer-Assisted Intervention–MICCAI 2006*, pp. 9–16, 2006.

[12] C. I. Christodoulou, C. S. Pattichis, M. Pantziaris, and A. Nicolaides, "Texture-based classification of atherosclerotic carotid plaques," *Medical Imaging, IEEE Transactions on*, vol. 22, no. 7, pp. 902–912, 2003.

[13] R. Sharma, R. B. Singh, and R. K. Gupta, "A segmentation method for carotid artery atherosclerosis plaque for MRI contrast and MRI features, oxidative stress markers in coronary and carotid plaque," in *Computer-Based Medical Systems, 2003. Proceedings. 16th IEEE Symposium*, 2003, pp. 323–328.

[14] K. W. Gossage, C. M. Smith, E. M. Kanter, L. P. Hariri, A. L. Stone, J. J. Rodriguez, S. K. Williams, and J. K. Barton, "Texture analysis of speckle in optical coherence tomography images of tissue phantoms," *Physics in Medicine and Biology*, vol. 51, p. 1563, 2006.

[15] M. Shiomi, T. Ito, S. Yamada, S. Kawashima, and J. Fan, "Development of an animal model for spontaneous myocardial infarction (WHHLMI rabbit)," *Arteriosclerosis, thrombosis, and vascular biology*, vol. 23, no. 7, pp. 1239–1244, 2003.

[16] T. Kobayashi, T. Ito, and M. Shiomi, "Roles of the WHHL Rabbit in Translational Research on Hypercholesterolemia and Cardiovascular Diseases," *Journal of Biomedicine and Biotechnology*, vol. 2011, pp. 1–10, 2011.

[17] A. Nasser Esgiar, R. N. Naguib, B. S. Sharif, M. K. Bennett, and A. Murray, "Microscopic image analysis for quantitative measurement and feature identification of normal and cancerous colonic mucosa," *Information Technology in Biomedicine, IEEE Transactions on*, vol. 2, no. 3, pp. 197–203, 1998.

[18] R. M. Haralick, K. Shanmugam, and I. H. Dinstein, "Textural features for image classification," *Systems, Man and Cybernetics, IEEE Transactions on*, no. 6, pp. 610–621, 1973.

[19] F. Argenti, L. Alparone, and G. Benelli, "Fast algorithms for texture analysis using co-occurrence matrices," in *Radar and Signal Processing, IEE Proceedings F*, 1990, vol. 137, pp. 443–448.

[20] B. Nielsen, F. Albregtsen, and H. E. Danielsen, "Low dimensional adaptive texture feature vectors from class distance and class difference matrices," *Medical Imaging, IEEE Transactions on*, vol. 23, no. 1, pp. 73–84, 2004.

[21] A. M. Mimino, *Deaths: Preliminary Data for 2008*. DIANE Publishing, 2011.

[22] J. J. Maciejko, *Atherosclerosis Risk Factors*. Amer. Assoc. for Clinical Chemistry, 2004.

[23]S. J. George and J. Johnson, *Atherosclerosis*. John Wiley & Sons, 2010.

[24]T. H. McConnell, *The Nature Of Disease: Pathology For The Health Professions*. Lippincott Williams & Wilkins, 2007.

[25] Y. J. Geng, *Curren Topics in Atherosclerosis Research*. Nova Publishers, 2005.

[26]D. Labarthe, *Epidemiology and Prevention of Cardiovascular Diseases: A Global Challenge*. Jones & Bartlett Learning, 2011.

[27] R. Stocker and J. F. Keaney, "Role of oxidative modifications in atherosclerosis," *Physiological reviews*, vol. 84, no. 4, pp. 1381–1478, 2004.

[28] R. Doll, R. Peto, J. Boreham, and I. Sutherland, "Mortality from cancer in relation to smoking: 50 years observations on British doctors," *British journal of cancer*, vol. 92, no. 3, pp. 426–429, 2005.

[29] M. K. Hong, P. A. Romm, K. Reagan, C. E. Green, and C. E. Rackley, "Effects of estrogen replacement therapy on serum lipid values and angiographically defined coronary artery disease in postmenopausal women," *The American journal of cardiology*, vol. 69, no. 3, pp. 176–178, 1992.

[30] T. H. McConnell, *The nature of disease: Pathology for the health professions*. Lippincott Williams & Wilkins, 2006.

[31] G. B. Mutangadura, "World Health Report 2002: Reducing Risks, Promoting Healthy Life: World Health Organization, Geneva, 2002, 250 pages, US $13.50, ISBN 9-2415-6207-2," *Agricultural Economics*, vol. 30, no. 2, pp. 170–172, 2004.

[32] S. MacMahon, R. Peto, J. Cutler, R. Collins, P. Sorlie, J. Neaton, R. Abbott, J. Godwin, A. Dyer, and J. Stamler, "Blood pressure, stroke, and coronary heart disease. Part 1, Prolonged differences in blood pressure: prospective observational studies corrected for the regression dilution bias.," *Lancet*, vol. 335, no. 8692, p. 765, 1990.

[33] U. D. of Health and H. Services, *Reducing the health consequences of smoking: 25 years of progress. A report of the surgeon general*. US Government Printing Office Washington^ eDC DC, 1989.

[34] M. Naghavi, P. Libby, E. Falk, S. W. Casscells, S. Litovsky, J. Rumberger, J. J. Badimon, C. Stefanadis, P. Moreno, G. Pasterkamp, Z. Fayad, P. H. Stone, S. Waxman, P. Raggi, M. Madjid, A. Zarrabi, A. Burke, C. Yuan, P. J. Fitzgerald, D. S. Siscovick, C. L. De Korte, M. Aikawa, K. E. Juhani Airaksinen, G. Assmann, C. R. Becker, J. H. Chesebro, A. Farb, Z. S. Galis, C. Jackson, I.-K. Jang, W. Koenig, R. A. Lodder, K. March, J. Demirovic, M. Navab, S. G. Priori, M. D. Rekhter, R. Bahr, S. M. Grundy, R. Mehran, A. Colombo, E. Boerwinkle, C. Ballantyne, W. Insull, R. S. Schwartz, R. Vogel, P. W. Serruys, G. K. Hansson, D. P. Faxon, S. Kaul, H. Drexler, P. Greenland, J. E. Muller, R. Virmani, P. M. Ridker, D. P. Zipes, P. K. Shah, and J. T. Willerson,

"From vulnerable plaque to vulnerable patient: a call for new definitions and risk assessment strategies: Part II.," *Circulation*, vol. 108, no. 15, pp. 1664–1672, 2003.

[35] R. Herdman, M. Hewitt, and M. Laschober, "Smoking-related deaths and financial costs: Office of Technology Assessment estimates for 1990," in *Washington, DC: Office of Technology Assessment, Congress of the United States*, 1993.

[36] M.-H. Tan and D. R. MacLean, "Epidemiology of diabetes mellitus in Canada.," *Clinical and investigative medicine. Medecine clinique et experimentale*, vol. 18, no. 4, p. 240, 1995.

[37] "Diabetes and Coronary Heart Disease," *New England Journal of Medicine*, vol. 339, no. 23, pp. 1714–1716, 1998.

[38] V. Bamba and D. J. Rader, "Obesity and Atherogenic Dyslipidemia," *Gastroenterology*, vol. 132, no. 6, pp. 2181–2190, May 2007.

[39] Z. Wang and T. Nakayama, "Inflammation, a Link between Obesity and Cardiovascular Disease," *Mediators of Inflammation*, vol. 2010, pp. 1–17, 2010.

[40] G. B. Mutangadura, "World Health Report 2002: Reducing Risks, Promoting Healthy Life: World Health Organization, Geneva, 2002, 250 pages, US $13.50, ISBN 9-2415-6207-2," *Agricultural Economics*, vol. 30, no. 2, pp. 170–172, 2004.

[41] N. Anastassopoulou, B. Arapoglou, P. Demakakos, M. I. Makropoulou, A. Paphiti, and A. A. Serafetinides, "Spectroscopic characterisation of carotid atherosclerotic plaque by laser induced fluorescence," *Lasers Surg Med*, vol. 28, no. 1, pp. 67–73, 2001.

[42]L. Marcu, J. A. Jo, Q. Fang, T. Papaioannou, T. Reil, J.-H. Qiao, J. D. Baker, J. A. Freischlag, and M. C. Fishbein, "Detection of Rupture-Prone Atherosclerotic Plaques by Time-Resolved Laser Induced Fluorescence Spectroscopy," *Atherosclerosis*, vol. 204, no. 1, pp. 156–164, May 2009.

[43] R. Rocha, A. B. Villaverde, L. Silveira, M. S. Costa, L. P. Alves, C. A. Pasqualucci, and A. Brugnera, "Identification of Atherosclerotic Plaques in Carotid Artery by Fluorescence Spectroscopy," *AIP Conference Proceedings*, vol. 992, no. 1, pp. 1151–1155, Apr. 2008.

[44] J. D. Caplan, S. Waxman, R. W. Nesto, and J. E. Muller, "Near-infrared spectroscopy for the detection of vulnerable coronary artery plaques," *J. Am. Coll. Cardiol.*, vol. 47, no. 8 Suppl, pp. C92–96, Apr. 2006.

[45] A. Hamdan, A. Assali, S. Fuchs, A. Battler, and R. Kornowski, "Imaging of vulnerable coronary artery plaques," *Catheterization and Cardiovascular Interventions*, vol. 70, no. 1, pp. 66–75, 2007.

[46] M. B. Lilledahl, O. A. Haugen, L. L. Randeberg, and L. O. Svaasand, "Characterization of atherosclerotic plaque by reflection spectroscopy and thermography: a comparison," pp. 415–425, Apr. 2005.

[47] P. R. Moreno and J. E. Muller, "Detection of high-risk atherosclerotic coronary plaques by intravascular spectroscopy," *J Interv Cardiol*, vol. 16, no. 3, pp. 243–252, Jun. 2003. R. Rocha, L. Silveira Jr, A. B. Villaverde, C. A. Pasqualucci, M. S. Costa, A. Brugnera Jr, and M. T. T. Pacheco, "Use of near-infrared Raman spectroscopy for identification of atherosclerotic plaques in the carotid artery," *Photomed Laser Surg*, vol. 25, no. 6, pp. 482–486, Dec. 2007.

[48] L. B. Mostaço-Guidolin, A. C.-T. Ko, D. P. Popescu, M. S. D. Smith, E. K. Kohlenberg, M. Shiomi, A. Major, and M. G. Sowa, "Evaluation of texture parameters for the quantitative description of multimodal nonlinear optical images from atherosclerotic rabbit arteries," *Phys Med Biol*, vol. 56, no. 16, pp. 5319–5334, Aug. 2011.

[50] M. E. Brezinski, *Optical coherence tomography: principles and applications*. Academic press, 2006.

[51] M. E. Brezinski, G. J. Tearney, B. E. Bouma, J. A. Izatt, M. R. Hee, E. A. Swanson, J. F. Southern, and J. G. Fujimoto, "Optical coherence tomography for optical biopsy. Properties and demonstration of vascular pathology," *Circulation*, vol. 93, no. 6, pp. 1206–1213, Mar. 1996.

[52] D. Huang, E. A. Swanson, C. P. Lin, J. S. Schuman, W. G. Stinson, W. Chang, M. R. Hee, T. Flotte, K. Gregory, and C. A. Puliafito, "Optical coherence tomography," Massachusetts Institute of Technology, Whitaker College of Health Sciences and Technology, 1993.

[53] J. G. Fujimoto, "Optical coherence tomography for ultrahigh resolution in vivo imaging," *Nat. Biotechnol.*, vol. 21, no. 11, pp. 1361–1367, Nov. 2003.

[54] J. G. Fujimoto, M. E. Brezinski, G. J. Tearney, S. A. Boppart, B. Bouma, M. R. Hee, J. F. Southern, and E. A. Swanson, "Optical biopsy and imaging using optical coherence tomography," *Nature medicine*, vol. 1, no. 9, pp. 970–972, 1995.

[55] F. J. van der Meer, D. J. Faber, M. C. G. Aalders, A. A. Poot, I. Vermes, and T. G. van Leeuwen, "Apoptosis- and necrosis-induced changes in light attenuation measured by optical coherence tomography," *Lasers Med Sci*, vol. 25, no. 2, pp. 259–267, Mar. 2010.

[56] N. A. Patel, D. L. Stamper, and M. E. Brezinski, “Review of the ability of optical coherence tomography to characterize plaque, including a comparison with intravascular ultrasound,” *Cardiovascular and interventional radiology*, vol. 28, no. 1, pp. 1–9, 2005.

[57] H. Yabushita, B. E. Bouma, S. L. Houser, H. T. Aretz, I.-K. Jang, K. H. Schlendorf, C. R. Kauffman, M. Shishkov, D.-H. Kang, E. F. Halpern, and G. J. Tearney, “Characterization of Human Atherosclerosis by Optical Coherence Tomography,” *Circulation*, vol. 106, no. 13, pp. 1640–1645, Sep. 2002.

[58] W. Drexler and J. G. Fujimoto, *Optical Coherence Tomography: Technology and Applications*. Springer, 2008.

[59] G. J. Tearney, S. A. Boppart, B. E. Bouma, M. E. Brezinski, N. J. Weissman, J. F. Southern, and J. G. Fujimoto, “Scanning single-mode fiber optic catheter-endoscope for optical coherence tomography,” *Optics Letters*, vol. 21, no. 7, pp. 543–545, 1996.

[60] M. E. Brezinski, G. J. Tearney, B. E. Bouma, J. A. Izatt, M. R. Hee, E. A. Swanson, J. F. Southern, and J. G. Fujimoto, “Optical coherence tomography for optical biopsy: properties and demonstration of vascular pathology,” *Circulation*, vol. 93, no. 6, pp. 1206–1213, 1996.

[61] G. J. Tearney, M. E. Brezinski, B. E. Bouma, S. A. Boppart, C. Pitris, J. F. Southern, and J. G. Fujimoto, “In vivo endoscopic optical biopsy with optical coherence tomography,” *Science*, vol. 276, no. 5321, pp. 2037–2039, 1997.

[62] B. E. Bouma and G. J. Tearney, “Power-efficient nonreciprocal interferometer and linear-scanning fiber-optic catheter for optical coherence tomography,” *Optics Letters*, vol. 24, no. 8, pp. 531–533, 1999.

[63] I.-K. Jang, B. E. Bouma, D.-H. Kang, S.-J. Park, S.-W. Park, K.-B. Seung, K.-B. Choi, M. Shishkov, K. Schlendorf, E. Pomerantsev, S. L. Houser, H. T. Aretz, and G. J. Tearney, “Visualization of coronary atherosclerotic plaques in patients using optical coherence tomography: comparison with intravascular ultrasound,” *J Am Coll Cardiol*, vol. 39, no. 4, pp. 604–609, Feb. 2002.

[64] T. Kume, T. Akasaka, T. Kawamoto, N. Watanabe, E. Toyota, Y. Neishi, R. Sukmawan, Y. Sadahira, and K. Yoshida, “Assessment of coronary intima-media thickness by optical coherence tomography,” *Circ J*, vol. 69, no. 903, p. 7, 2005.

[65] W. Drexel, J. G. Fujimoto, and P. Gueye, “Optical Coherence Tomography Technology and Applications,” *Medical Physics*, vol. 36, p. 4842, 2009.

[66] F. D. Kolodgie, R. Virmani, A. P. Burke, A. Farb, D. K. Weber, R. Kutys, A. V. Finn, and H. K. Gold, “Pathologic assessment of the vulnerable human coronary plaque,” *Heart*, vol. 90, no. 12, pp. 1385–1391, 2004.

[67] R. Virmani, F. D. Kolodgie, A. P. Burke, A. Farb, and S. M. Schwartz, "Lessons from sudden coronary death a comprehensive morphological classification scheme for atherosclerotic lesions," *Arteriosclerosis, thrombosis, and vascular biology*, vol. 20, no. 5, pp. 1262–1275, 2000.

[68] H. M. Loree, A. J. Grodzinsky, S. Y. Park, L. J. Gibson, and R. T. Lee, "Static circumferential tangential modulus of human atherosclerotic tissue," *Journal of biomechanics*, vol. 27, no. 2, pp. 195–204, 1994.

[69] G. J. Tearney, I.-K. Jang, and B. E. Bouma, "Optical coherence tomography for imaging the vulnerable plaque," *Journal of biomedical optics*, vol. 11, no. 2, pp. 021002–021002, 2006.

[70] G. J. Tearney and B. E. Bouma, "Atherosclerotic plaque characterization by spatial and temporal speckle pattern analysis," *Optics letters*, vol. 27, no. 7, pp. 533–535, 2002.

[71] A. J. Martin, L. K. Ryan, A. I. Gotlieb, R. M. Henkelman, and F. S. Foster, "Arterial imaging: comparison of high-resolution US and MR imaging with histologic correlation," *Radiographics*, vol. 17, no. 1, pp. 189–202, Feb. 1997.

[72] J. M. Tobis, J. Mallery, D. Mahon, K. Lehmann, P. Zalesky, J. Griffith, J. Gessert, M. Moriuchi, M. McRae, and M. L. Dwyer, "Intravascular ultrasound imaging of human coronary arteries in vivo. Analysis of tissue characterizations with comparison to in vitro histological specimens," *Circulation*, vol. 83, no. 3, pp. 913–926, Mar. 1991.

[73] F. Prati, E. Arbustini, A. Labellarte, B. Dal, L. Sommariva, M. Mallus, A. Pagano, and A. Boccanelli, "Correlation between high frequency intravascular ultrasound and histomorphology in human coronary arteries," *Heart*, vol. 85, no. 5, pp. 567–570, May 2001.

[74] J. A. Rumberger, T. Behrenbeck, J. F. Breen, and P. F. Sheedy 2nd, "Coronary calcification by electron beam computed tomography and obstructive coronary artery disease: a model for costs and effectiveness of diagnosis as compared with conventional cardiac testing methods," *J. Am. Coll. Cardiol.*, vol. 33, no. 2, pp. 453–462, Feb. 1999.

[75] N. D. Wong, A. Vo, D. Abrahamson, J. M. Tobis, H. Eisenberg, and R. C. Detrano, "Detection of coronary artery calcium by ultrafast computed tomography and its relation to clinical evidence of coronary artery disease," *Am. J. Cardiol.*, vol. 73, no. 4, pp. 223–227, Feb. 1994.

[76] M. J. Budoff and B. H. Brundage, "Electron beam computed tomography: screening for coronary artery disease," *Clin Cardiol*, vol. 22, no. 9, pp. 554–558, Sep. 1999.

[77] M. Naghavi, M. Madjid, M. R. Khan, R. M. Mohammadi, J. T. Willerson, and S. W. Casscells, "New developments in the detection of vulnerable plaque," *Curr Atheroscler Rep*, vol. 3, no. 2, pp. 125–135, Mar. 2001.

[78] F. M. Baer, P. Theissen, C. A. Schneider, K. Kettering, E. Voth, U. Sechtem, and H. Schicha, "MRI assessment of myocardial viability: comparison with other imaging techniques," *Rays*, vol. 24, no. 1, pp. 96–108, Mar. 1999.

[79] B. D. MacNeill, H. C. Lowe, M. Takano, V. Fuster, and I. K. Jang, 'Intravascular Modalities for Detection of Vulnerable Plaque Current Status', *Arteriosclerosis, thrombosis, and vascular biology*, vol. 23, no. 8, pp. 1333–1342, 2003.

[80] I. K. Jang, B. E. Bouma, D. H. Kang, S. J. Park, S. W. Park, K. B. Seung, K. B. Choi, M. Shishkov, K. Schlendorf, and E. Pomerantsev, 'Visualization of coronary atherosclerotic plaques in patients using optical coherence tomography: comparison with intravascular ultrasound', *Journal of the American College of Cardiology*, vol. 39, no. 4, pp. 604–609, 2002.

[81] K. W. Gossage, T. S. Tkaczyk, J. J. Rodriguez, and J. K. Barton, 'Texture analysis of optical coherence tomography images: feasibility for tissue classification', *Journal of biomedical optics*, vol. 8, no. 3, pp. 570–575, 2003

[82] C. I. Christodoulou, C. S. Pattichis, M. Pantziaris, and A. Nicolaides, 'Texture-based classification of atherosclerotic carotid plaques', *Medical Imaging, IEEE Transactions on*, vol. 22, no. 7, pp. 902–912, 2003.

[83] A. P. Dhawan, Y. Chitre, and C. Kaiser-Bonasso, 'Analysis of mammographic microcalcifications using gray-level image structure features', *Medical Imaging, IEEE Transactions on*, vol. 15, no. 3, pp. 246–259, 1996.
[80] C. M. Wu, Y. C. Chen, and K. S. Hsieh, 'Texture features for classification of ultrasonic liver images', *Medical Imaging, IEEE Transactions on*, vol. 11, no. 2, pp. 141–152, 1992.

[84] J. K. Kim and H. W. Park, 'Statistical textural features for detection of microcalcifications in digitized mammograms', *Medical Imaging, IEEE Transactions on*, vol. 18, no. 3, pp. 231–238, 1999.

[85] A. Rosenfeld and E. Troy, "Visual texture analysis," Tech. Rep. 70-116, University of Maryland, College Park, MD, June 1970.

[86] R. M. Haralick, K.,S. Shanmugam, au.d I. Dinstein, "Textural features for image classification," IEEE fl-a,fl' Syst., Man, Gybern., vol. SMC-3, no. 6, pp. 610-621, 1973.

[87] A. Nasser Esgiar, R. N. G. Naguib, B. S. Sharif, M. K. Bennett, and A. Murray, 'Microscopic image analysis for quantitative measurement and feature identification of

normal and cancerous colonic mucosa', *Information Technology in Biomedicine, IEEE Transactions on*, vol. 2, no. 3, pp. 197–203, 1998.

[88] R. M. Haralick, K. Shanmugam, and I. H. Dinstein, 'Textural features for image classification', *Systems, Man and Cybernetics, IEEE Transactions on*, no. 6, pp. 610–621, 1973.

[89] F. Argenti, L. Alparone, and G. Benelli, 'Fast algorithms for texture analysis using co-occurrence matrices', in *Radar and Signal Processing, IEE Proceedings F*, 1990, vol. 137, pp. 443–448.

[90] B. Nielsen, F. Albregtsen, and H. E. Danielsen, 'Low dimensional adaptive texture feature vectors from class distance and class difference matrices', *Medical Imaging, IEEE Transactions on*, vol. 23, no. 1, pp. 73–84, 2004.

[91] A. Fisher, "The mathematical theory of probabilities," Vol.1, New York, 1923.

[92] K. Fukunaga, *Introduction to Statistical Pattern Recognition*, Academic Press, 1990.

[93] H.-P. Kriegel, A. Pryakhin, and M. Schubert, "Multi-represented kNN-classification for large class sets," in *Database Systems for Advanced Applications*, 2005, pp. 511–522.

[94] P. E. Hart and D. G. Stork, "Pattern classification," *John Willey & Sons*, 2001.

[95] P. A. Lachenbruch and M. R. Mickey, "Estimation of error rates in discriminant analysis," *Technometrics*, vol. 10, no. 1, pp. 1–11, 1968.

[96] K. W. Gossage, T. S. Tkaczyk, J. J. Rodriguez, and J. K. Barton, "Texture analysis of optical coherence tomography images: feasibility for tissue classification," *Journal of biomedical optics*, vol. 8, no. 3, pp. 570–575, 2003.

[97] J. S. Weszka, C. R. Dyer, and A. Rosenfeld, 'A comparative study of texture measures for terrain classification', *Systems, Man and Cybernetics, IEEE Transactions on*, no. 4, pp. 269–285, 1976.

[99] M. M. Galloway, 'Texture analysis using gray level run lengths', *Computer graphics and image processing*, vol. 4, no. 2, pp. 172–179, 1975.

[100] G. G. Lendaris and G. L. Stanley, 'Diffraction-pattern sampling for automatic pattern recognition', *Proceedings of the IEEE*, vol. 58, no. 2, pp. 198–216, 1970.

[101] R. W. Conners and C. A. Harlow, 'A theoretical comparison of texture algorithms', *Pattern Analysis and Machine Intelligence, IEEE Transactions on*, no. 3, pp. 204–222, 1980.

[102] E. Brunenberg, O. Pujol, B. ter Haar Romeny, and P. Radeva, 'Automatic IVUS segmentation of atherosclerotic plaque with stop & go snake', *Medical Image Computing and Computer-Assisted Intervention–MICCAI 2006*, pp. 9–16, 2006.

[103] D. Vukadinovic, S. Rozie, M. van Gils, T. van Walsum, R. Manniesing, A. van der Lugt, and W. J. Niessen, 'Automated versus manual segmentation of atherosclerotic carotid plaque volume and components in CTA: associations with cardiovascular risk factors', *Int J Cardiovasc Imaging*, vol. 28, no. 4, pp. 877–887, Apr. 2012.

[104] V. Amirbekian, M. J. Lipinski, K. C. Briley-Saebo, S. Amirbekian, J. G. S. Aguinaldo, D. B. Weinreb, E. Vucic, J. C. Frias, F. Hyafil, V. Mani, E. A. Fisher, and Z. A. Fayad, "Detecting and assessing macrophages in vivo to evaluate atherosclerosis noninvasively using molecular MRI," *PNAS*, vol. 104, no. 3, pp. 961–966, Jan. 2007.

[105] J. A. Hartigan and M. A. Wong, 'Algorithm AS 136: A k-means clustering algorithm', *Applied statistics*, pp. 100–108, 1979.